

# The GR model

## Somme special information about GR model

### The problem of DAC and BAL phenomena in the UV spectra of Hot Emission Stars and Quasars respectively.

E. Danezis, E. Lyratzi, A. Antoniou, D. Stathopoulos, D. Tzimeas  
Astrophysical Spectroscopy Team  
National and Kapodistrian University of Athens

#### DACs and SACs structure

An important characteristic of hot stars (i.e. stars with effective temperatures  $\geq 10000$  K) is that they lose mass via a stellar wind. One of the most sensitive diagnostics of these stellar winds comes from high resolution UV spectroscopy. The UV spectra of hot stars reveal extended, velocity displaced P-Cygni type profiles in various objects, including the following (Prinja 1990):

- WR stars (Willis et al. 1986; Willis and Garmany 1987),
- OB stars (e.g. Garmany et al. 1981; Gathier et al. 1981; Prinja and Howarth, 1986),
- subdwarf O stars (e.g. Heap et al. 1979, Simon et al. 1979),
- the central stars of planetary nebulae (CSPN; e. g. Heap 1986, Pauldrach et al. 1988),
- Be stars (e.g. Snow 1981; Grady et al. 1987; Danezis, E. et al. 2003a; Lyratzi, et al. 2007; Danezis et al. 2009; Antoniou et al. 2011a, 2011b),
- Oe stars (Antoniou et al. 2007a, 2007b, 2007c, 2007d, 2008, 2014; Danezis et al. 2003a, 2003b, 2007; Danezis et al. 2009)

Other astronomical objects that exhibit P-Cygni type line profiles are cataclysmic variables (CVs), young stellar objects (YSOs) and AGN (Proga et al. 2002, Proga 2005).

CVs exhibit absorption troughs extending blueward over 5000 km/s. This phenomenon is attributed to high-velocity winds by analogy with OB stars (e.g., Krautter et al. 1981). However, observationally, the P-Cygni profiles of CVs differ from the profiles of early-type stars in two significant ways: First, whereas the deepest part of the blueshifted absorption component of the line profiles of early-type stars is near the terminal velocity, the deepest part of the line profiles of CVs is near zero velocity. Second, the absorption components of the line profiles of early-type stars are often are black, whereas in CVs they are at most roughly half the depth of the continuum. As judged by the velocity of the blue edge of the absorption component of the profiles, the terminal velocity of the wind is roughly 5000 km/s (Mauche & Raymond 1997).

Data reveal maximum wind velocities  $> 1000$  km/s (far in excess of the photospheric escape velocities). The most accepted theory behind the winds of hot stars is the one based on radiation pressure driving, but there are still big

questions to be answered. For example the extent to which radiation pressure provides the dominant force in the winds of various classes of hot stars is undetermined, and other mechanisms might play an important role, for example, in cooler, less luminous objects such as late B and B (emission) stars (Prinja 1990).

Among the class of hot stars there are two subsets of stars, i.e. Be and Oe, with a special spectral characteristic. Bidelman and Svolopoulos (1960) detected hydrogen emission and shell lines on spectrograms taken in 1959 and classified the object as a Be star. Classical Be stars are a rapidly rotating subset of non-giant B-type [17% of B-type stars are Be stars (Zorec & Briot 1997)] stars. Unlike normal B-type stars, Be stars exhibit line emission (hence the 'e' in Be), which is attributed to a gaseous circumstellar disk in Keplerian motion (Labadie-Bartz et al. 2017). A normal B star does not show emission lines, when it is in the main sequence. It does so when it is a supergiant (Vardya et al. 1982). The central stars rotate close to break-up velocities, and an uncertain mechanism – the so-called Be phenomenon – acts in addition to rotation, leading to episodic or continuous mass ejection from the stellar equator. Subsequently, outflowing, ionised, purely gaseous disks, rotating in a nearly Keplerian way are formed (Klement et al. 2017). A recent review is provided by Rivinius et al. 2013. The circumstellar disk of a Be star is best described by the viscous decretion disk model (e.g. Lee et al. 1991; Carciofi 2011), where the disk is formed and subsequently sustained by mass ejected from the stellar surface in discrete events called 'outbursts' (e.g. Kroll & Hanuschik (1997) or Kee et al. (2014) for a theoretical framework, or Rivinius et al. (1998) or Grundstrom et al. (2011) for observations).

The optical emission lines are generally more or less symmetric, with the center of the emission placed at or near the stellar rest wavelength, showing that within the Balmer emission envelope the expansion velocity is  $\lesssim 1000 \text{ km/s}$  (Barker & Marlborough 1985). On the other hand the resonance doublets of transitions such as N V, C IV and Si IV which are present in the UV spectra of Be stars exhibit extended shortward absorption and asymmetry. These characteristics indicate high velocity ( $\gtrsim 1000 \text{ km/s}$ ) mass loss via a stellar wind (Barker & Marlborough 1985). These species are called "superionized" because even at the high effective temperatures of Be stars, these ions are not expected to exist in sufficient abundance to produce observable features under radiative equilibrium conditions (Lamers & Snow 1978).

Ultraviolet observations of Be/Shell stars with IUE indicated the presence of highly ionized spectral lines than normal B type stars, C IV and Si IV are detected. UV spectra of Be/Shell stars reveal short ward velocity shifts up to 1300 km/s, suggesting the expansion of the circumstellar material away from the stars, Slettebak, (1988). The C IV doublet is of great importance as it is observed in Be stars as late as B9, yet among normal (no H $\alpha$  emission) B stars, C IV is only observed at B2 or earlier (Barker et al. 1984).

The class of Oe stars was defined by Conti & Leep (1974) as O stars displaying emission lines of the H I Balmer series as well as of lower ionization elements such as He II and Fe II, but that do not show typical Of emission lines such as He II  $\lambda$  4686 and N III  $\lambda$  4634-40. These stars were commonly considered to be massive analogs of Be stars and they seemed to form an extension of the Be phenomenon towards higher stellar temperatures. However, Negueruela et al. (2004) revised the spectral types of most Oe stars, arguing that previous classifications were too early because of infilling of the He I lines. Most Oe stars would thus have true spectral types in the range O9–B0 (the earliest member of the Oe category is the O7.5 IIIe star HD155806, Negueruela et al. 2004). Oe stars exhibit double-peaked or central emission in their Balmer lines. This emission-line morphology is distinct from signatures of stellar winds, and is conventionally attributed to a circumstellar disk. Although Oe stars are usually considered to be a continuation of the Be phenomenon toward hotter spectral types, it is difficult to understand how stable disks can coexist with the increasingly strong stellar winds typical of O-type stars. A plausible explanation is that the disk is maintained by a large-scale (e.g., dipolar) magnetic field that channels outflowing wind material toward the magnetic equator, in which case the disk and the wind are really a single entity (Fullerton et al. 2011).

One of the most striking features in the spectra of hot star winds is the presence of Discrete Absorption Components (DACs). These DACs are superimposed on the absorption troughs of unsaturated resonance line P-Cygni profiles in the UV spectra of OB stars, and move from the lower blue-shift to higher blue-shift part of P-Cygni profiles (e.g. Prinja & Howarth 1988; Massa et al. 1995; Kaper et al. 1997; Prinja et al. 2002). These stellar wind features are evident as narrow (FWHM  $\sim$  100-300 km/s) opacity enhancements which typically occur at  $\sim$ 0.5-0.9 of the maximum observed wind velocity (Prinja 1990). They are usually attributed to the presence of large scale structures leading to optical depth enhancement. These spectral features often dominate the profiles and are interpreted as observational evidence for the inhomogeneous, non-spherical and non-laminar nature of these winds.

The resonance lines which are most sensitive indicators of mass-loss include N V, Si IV, C IV and Mg II. These features are identified when they occur at the same velocity in both members of a resonance doublet (see Figs. 1, 2). We need to note that in Fig. 2 there are cases such as HD 32991 and HD 11158 where the entire stellar wind may be observed only in the form of discrete absorption components, without the absence of an underlying P-Cygni profile.

The mechanisms responsible for the creation of DACs are an important problem that has been studied by many researchers. Some have suggested mechanisms that allow the existence of structures which cover all or a significant part of the stellar disk, such as shells, blobs or puffs (Underhill 1975, Henrichs 1984, Underhill & Fahey 1984, Bates & Halliwell 1986, Grady et al. 1987, Lamers et al. 1988, Waldron et al. 1992, 1994, Cranmer & Owocki 1996, Rivinius et al.

1997, Kaper et al. 1996, 1997, 1999, Markova 2000), interaction of fast and slow wind components, Co-rotating Interaction Regions (CIRs), structures due to magnetic fields or spiral streams as a result of the stellar rotation (Cranmer & Owocki 1996, Kaper et al. 1996, 1997, 1999, Mulan 1984a, b, 1986, Prinja & Howarth 1988, Fullerton et al. 1997, Cranmer et al. 2000). According to these ideas, DACs result from independent high density regions in the stellar environment, which have different rotational and radial velocities.

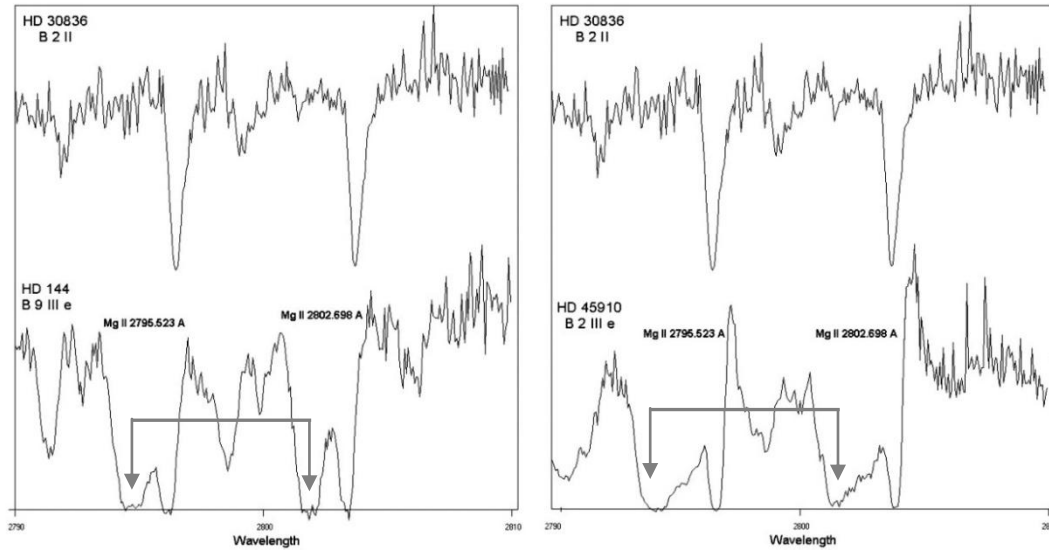


Figure 1. Comparison of the Mg II resonance lines between the spectrum of a normal B star and the spectra of two active Be stars that present complex and peculiar spectral lines. As we can observe the Be stars present some absorption components that do not appear in the spectrum of the classical B star (Danezis et al. 2010).

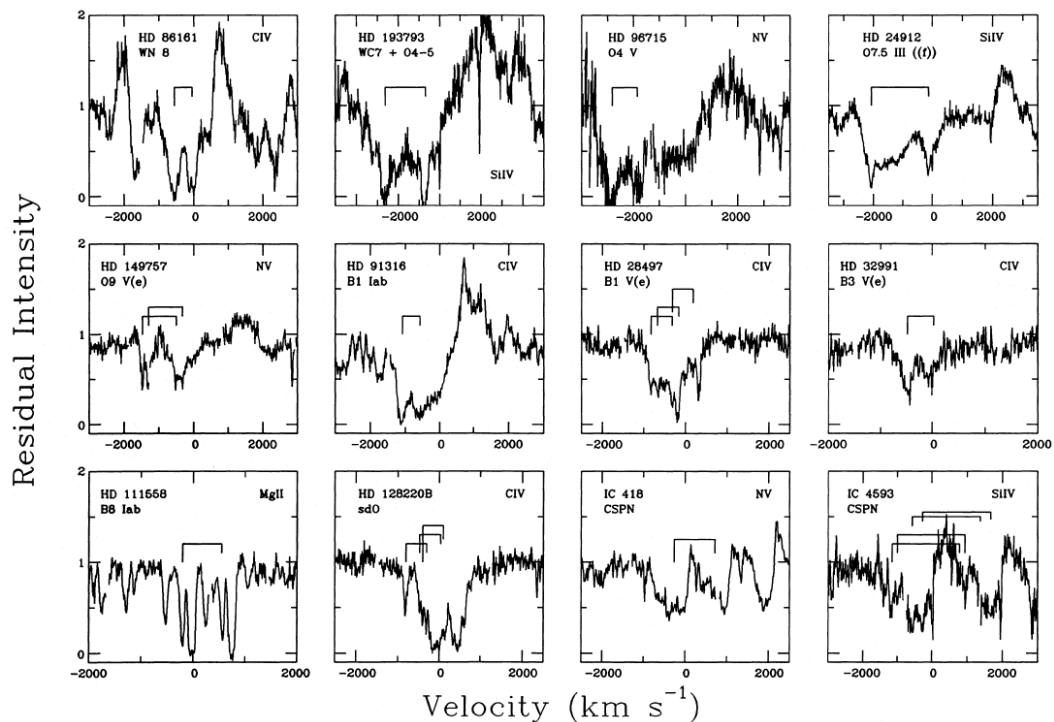


Figure 2. IUE spectra illustrating DACs in WR, O, B, Be, SdO and CSPN stars (Prinja 1990).

However, DACs are not unknown absorption spectral lines, but spectral lines of the same ion and the same wavelength as a main spectral line, shifted at different  $\Delta\lambda$ , as they are created in different density regions which rotate and move radially with different velocities (Danezis 1983, 1987, 1991, 2003, Lyratzi & Danezis 2004).

Another problem which is usually observed in the spectra of hot stars is that DACs exhibit very complex profiles and can't be reproduce theoretically with a single distribution, such as Gauss, Voigt, or Lorentz. In order to explain these complex line profiles Danezis et al. (2003, 2007a) and Lyratzi & Danezis 2004, Lyratzi et al. 2007a proposed the phenomenon of SACs (Satellite Absorption Components).

According to this phenomenon, a DAC is not a single absorption line, but the synthesis of a group of classical absorption components of the same spectral line of an ion (Satellite Absorption Components-SACs). These spectral components are formed in independent density regions (clumps) inside the turbulent stellar wind. If the independent density regions (clumps), that construct the Satellite Absorption Components of a DAC, rotate with large velocities and are close in velocity space, then they overlap forming a complex profile. More specifically, the absorption components are blended among themselves as well as with the main spectral line and thus they are not discrete but form a continuous complex profile (Danezis 1983, 1987, Lyratzi & Danezis 2004, Danezis et al. 2003, 2006, 2007a Sahade et al. 1984, Sahade & Brandi 1985). So, DACs and SACs are two aspects of the same phenomenon. In Fig. 2 it is clear that the Mg II line profiles of the star AX Mon (HD 45910), which presents DACs and the star HD 41335, which presents SACs are produced in the same way. The only difference between them is that the components of HD 41335 are much closer in velocity space and thus they overlap.

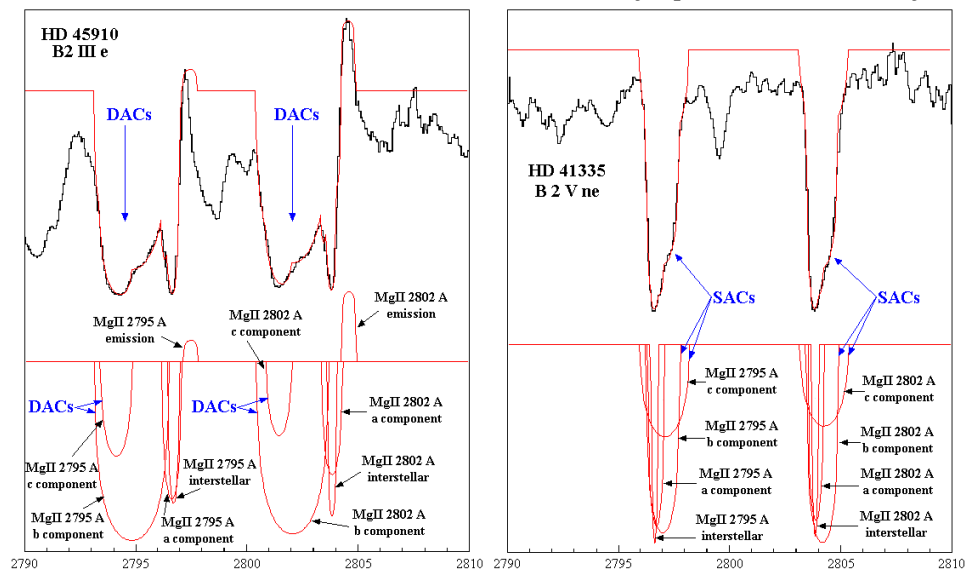


Figure 3. DACs of the Mg II line profiles of the Be star AX Mon (HD 45910) and SACs of the Be star HD 41335 are produced in the same way. The black line denotes the observed profile and the red one the model's fit. All the components which contribute to the observed features are shown below the fits (Danezis et al. 2009).

## From smooth wind models to «clumping» structure

O and B stars exhibit resonance lines from transitions such as C III, C IV, Si IV, N V with P-Cygni type profiles. The deepest part of the absorption profile corresponds to a velocity away from the star of  $\sim 1400$  km/s (Hearn, 1979). The absorption reaches a terminal velocity of  $\sim 1000$ - $3000$  km/s (Hearn 1981, Drechsel & Rahe, 1982). Because these speeds are much larger than the escape velocities from the surfaces of these stars, it is clear that the material escapes from them (Hearn, 1979), in the form of a wind.

It is believed that the winds of hot stars are produced through radiation pressure exerted via the interaction of ultraviolet (UV) photons with electrons bound to atoms in the stellar atmosphere (Lucy & Solomon 1970).

Castor, Abott & Klein (1975, hereafter CAK) created a theoretical wind model and showed that the wind and mass loss are driven by radiation forces which are related to resonance lines from ions such as C III, C IV, Si IV. CAK theory is a modification of Parker's model (Parker 1958) with an extra force due to radiation forces. Further modifications of the CAK theory included even more elaborate line lists (Abbott 1982a) and the inclusion of a finite disk correction factor, which allowed photons to stream from the entire stellar disk instead of only radially (Friend & Abbott 1986, Pauldrach et al. 1986). Additionally, occupation numbers were calculated in non-LTE (Pauldrach et al. 1994), further refining the theory (Vink 2009).

The basic properties of these modern-era CAK-like wind models are the following: the wind is assumed to be spherically symmetric, and homogeneous, i.e. clumps are not taken into account. However, wind variability is a well-known phenomenon both observationally as well as theoretically (see Wolf et al. 1998 for an overview). Furthermore, the emission of X-rays for single O stars (Harnden et al. 1979) as well as the presence of black troughs in UV P-Cygni line profiles indicate that the winds of O stars are not smooth. According to Owocki (1990), there are strong reasons, both observational and theoretical, for believing that hot star winds are not smooth, but rather are both spatially and temporally high variable. Observational evidence includes superionization, X-ray emission, Discrete Absorption Components (DACs) in unsaturated UV lines. The winds of O and B stars, which are manifested through UV P-Cygni profiles, present variability in timescales from several days to hours [e.g. Henrichs (1984) and Prinja & Howarth (1986)]. Time-resolved series of high-resolution UV spectra, obtained with the International Ultraviolet Explorer (IUE), have shown that the variations in UV resonance lines are not chaotic, but occur in well-defined "patterns" (e.g. Henrichs (1984); Prinja & Howarth (1986); Prinja et al. 1987, Henrichs et al. 1988) which are usually observed in Discrete Absorption Components (DACs).

It was mainly high-S/N, time-dependent spectroscopy of strong optical recombination emission lines in WR, and also a few OB and other stars with

strong hot winds, that indicated all hot stellar winds likely to be pervaded by thousands of multiscale (compressible supersonic turbulent?) structures, whose driver is probably some kind of radiative instability (Moffat 2008).

The theory of instabilities of radiatively driven stellar wind was introduced by Lucy & Solomon (1970) and was further developed by Lucy (1984), Owocki & Rybicki (1985, 1986, 1991), and extended to three-dimensional perturbations by Rybicki et al. (1990). Nelson & Hearn (1978), Martens (1979) and Mc Gregor et al. (1979) suggested that the flow is unstable against the radiatively driven instabilities. These instabilities will break up the flow destroying the balance between the forces and the result will be either to heat a corona or to set up the system of radiative driven blobs suggested by Lucy and White (1980) or both.

Between 1978 and 1995 when it was active, IUE satellite led to great strides in the field of hot-star winds, leading to the discovery, mostly in strong resonant lines, of large scale wind structures. These were referred to as discrete absorption components (DACs), seen mainly in the absorbing column between the observer and the projected disk of the star (Moffat 2008). Their variation with time (more or less periodically) is commonly believed to be due to large-scale co-rotating interactive regions (CIR), as seen in the Solar wind. In hot-star winds, CIRs are probably produced by some kind of rotating inhomogeneity at the surface of the star: non-radial pulsations or local magnetic loops come to mind, which then perturb the rotating wind (e.g. Cranmer & Owocki 1996). It is possible that all hot-star winds contain CIRs (Moffat, 2008).

According to Runacres & Owocki 2002 since the acceleration of the wind is a highly unstable process, it leads to strong irregularities in density and velocity. These irregularities, often referred to as clumps, have an impact on the observables of massive star winds, in particular affecting measured mass-loss rates. The characteristics of clumps are uncertain, but it is thought that they carry most of the wind mass, but fill only a small fraction ( $f < 1$ ) of the volume in the stellar surroundings, yielding a contrast of  $f^{-1}$  in density with respect to its average value (Bosch-Ramon 2013). The clump sizes are expected to be much smaller than the star (Owocki & Cohen 2006), although larger clumps may also be present in the wind like the clumps used, for instance, to explain the X-ray flares in supergiant fast X-ray transients (e.g. Walter & Zurita Heras 2007), or the large scale structures behind the observed discrete absorption components in the UV in early-type stars (DACs) (e.g. Cranmer & Owocki 1996; Lobel & Blomme 2008). The clumps should present a distribution of masses and sizes if they are the product of non-linear processes at the wind base (Moffat 2008).

But what now is normally referred to as clumping in hot-star winds is something that appears to be much more widespread and pervasive in all hot star winds than DACs/ CIRs. While many different phenomena pointed towards the presence of some kind of granulation in the winds, it took high-S/N, moderately-high time-resolved spectroscopy as the final clue to say that virtually all parts of all hot star winds are stochastically inhomogeneous on various

(mainly small) scales Moffat, 2008). This was first revealed in time-resolved optical spectra of WR stars, where their strong, broad emission lines probe the whole wind simultaneously, not just the column along the line-of-sight (Moffat, 2008).

Possibly the most convincing evidence for clumpy structures in hot-star winds comes from time resolved spectroscopic monitoring of WR emission lines (Schumann & Seggewiss). These now well-known spectral series show clear stochastic subpeaks of various sizes moving in a direction from line centre to line edge, interpreted as wind clumps whose projected velocities we see as they propagate with the outflow. Although the stars are not resolved, one reaches effectively a poor-man's resolution with the aid of Doppler expansion of the wind, which cannot unambiguously locate the structures other than in a ring of constant angle from the central star. Nevertheless, this was the first time that it became clear that small-scale wind structures are essentially universal at least in the strong winds of WR stars.

Besides the observations in the visible and UV region of the spectrum the strong X-ray flow, observed in O and B stars cannot be obtained by a smooth, steady and cold wind, so the model of normal winds [SSCW proposed by Friend & Abbott (1986) και Pauldrach et al. (1986)] is far from the true nature of the hot star winds (Vilkoviskij et al. 2003). So this model should be replaced by a more adequate model of an unstable and changing wind structures.

Although the easiest, most obvious results have emerged for "classical" WR stars because of their intense, broad emission lines, it is now clear that virtually all hot-star winds likely show similar effects.

As previously mentioned, Proga (2002) indicated that cataclysmic variables (CVs), young stellar objects (YSOs) and AGN share the similarity of exhibiting P-Cygni type profiles, mainly in their UV spectra. Proga (2007) points out that UV driven disk winds in AGN are motivated by analogy with winds from hot stars, which have been explored in great detail. Other researchers who have noticed similarities between the spectra of hot stars and AGN are:

- Woo (2013), who states that one of the prominent features for quasars is the BEL spectrum that is not seen except in the hottest stars. According to Woo (2013) Together with the emission features are broad absorption lines (BALs) which appear in at least 10% of optically-selected quasars. They are characterized by distinctive absorption troughs arising from resonance lines of various ions and they are blueshifted (outflowing) with respect to their associated BELs. There is general agreement that they are intrinsic to the quasar and caused by gas within the quasar itself, with outflow velocities up to thirty and possibly sixty thousand kilometers per second relative to the emission line redshift. Some are often described as P Cygni profiles, by analogy to similar features seen in stars which eject material toward the observer. Our understanding of the ability of the line-driving mechanism to produce powerful high-velocity winds is based on studies of

winds in hot stars that radiate mostly in the UV continuum. By analogy with O-stars, the presence of strong blueshifted absorption together with an intense UV radiation field suggests that radiation pressure acting on resonance lines is the acceleration mechanism (e.g., Lamers & Cassinelli 1999, and references therein). The presence of the BALs themselves strongly indicates that substantial momentum is transferred from a powerful radiation field to the outflowing wind. With the inclusion of resonance lines, Castor et al. (1975, hereafter CAK75) showed that the effective line-driven radiation force can increase by several orders of magnitude above that due to electron scattering alone.

- Feldmeier & Shlosman (1999) who state that observational signatures of line driven winds have been unambiguously detected in cataclysmic variables (CVs) and in active galactic nuclei. Observational evidence in favor of LDWs from hot stars and disks includes but is not limited to the P Cygni line profiles of C IV, N V and Si IV, ionization levels, high terminal velocities and their correlation with the luminosity.
- Danezis et al. (2006, 2008, 2010a, 2010b) indicated the analogies between the spectra of hot emission stars and BAL quasars. They applied their model and studied Si IV, C IV, and Mg II absorption profiles in the spectra of a number of hot emission stars and BALQSOs. They showed that in both types of astronomical objects, the broad and complex absorption troughs of Si IV, C IV and Mg II are the synthesis of individual absorbing components which are formed in independent absorbing regions (clouds, clumps) inside the outflow. They also showed that the outflows are far from being smooth but are clumpy and inhomogeneous (for some examples see Fig. 4).

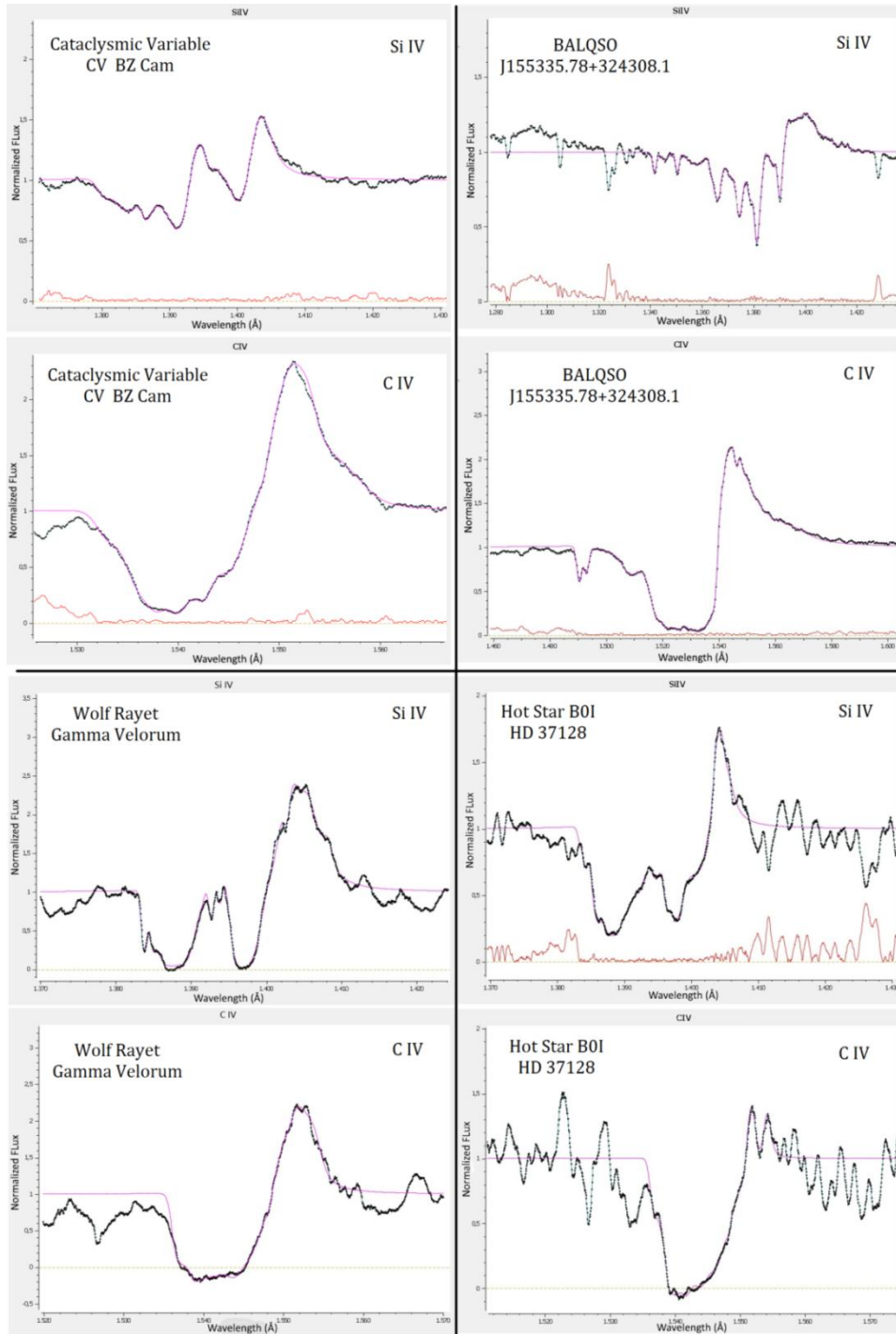


Figure 4. DAC/SAC phenomenon in the spectra of Hot Emission Stars, BAL Quasars, Cataclysmic Variables and Wolf Rayet stars.

## BAL structure in Quasar's spectra

In the spectra of about 10-20 % of the quasar population, in the UV region of the electromagnetic spectrum, we can observe Broad Absorption Lines (BALs), usually blueshifted with respect to the corresponding emission lines.

Quasars exhibiting this phenomenon are called Broad Absorption Line Quasars or BALQSOs (Foltz et al. 1990; Hewett & Foltz 2003; Reichard et al. 2003). BALs have very complex profiles and their blueshifts imply outflow velocities from near 0 to about 60,000 km/s (0.2c), (Foltz et al. 1983). BALQSO spectra present absorption in high level of ionization and transitions of C IV, N V, O VI, as well as absorption lines from transitions such as Si IV and Ly $\alpha$ . These QSOs are called High ionization BALQSOs or HiBALQSOs.

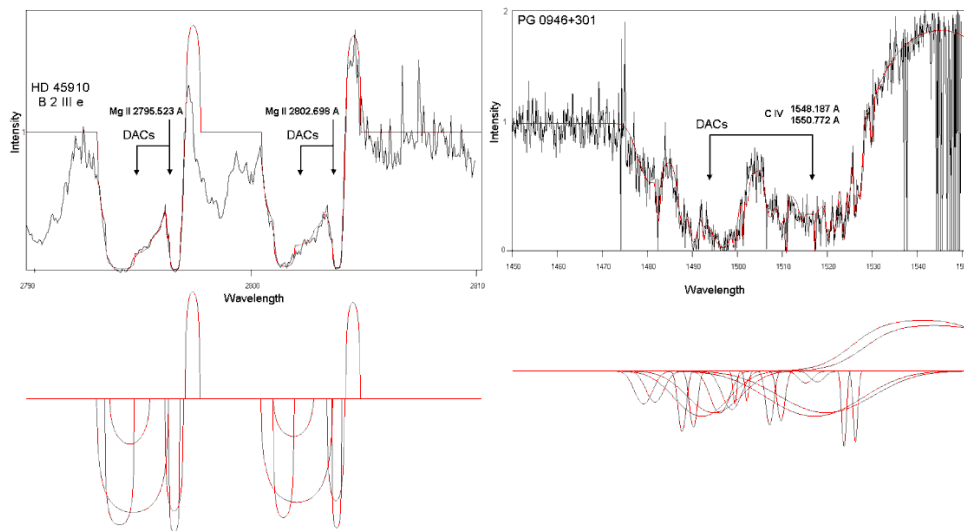


Figure 5. DACs phenomena (BAL) in AGNs spectra: Similarity of DACs phenomenon in Be star's HD 45910 spectrum (Mg II doublet) with AGNs PG 0946+301 spectrum (C IV doublet). In the case of the C IV doublet, the two discrete features do not correspond to the two resonance lines, as the two members of the doublet have small difference in wavelength (1548.187 Å and 1550.772 Å) and they both lie at the right feature.

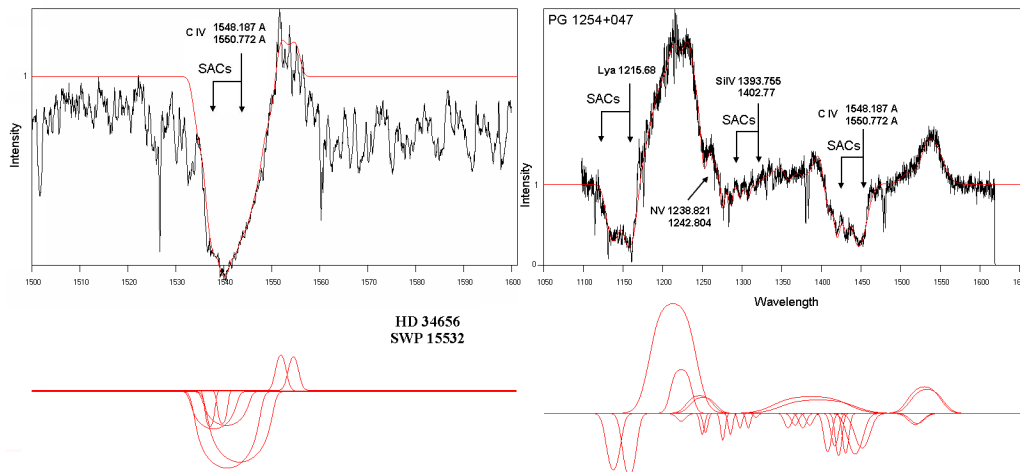


Figure 6. SACs phenomena in AGNs spectra: Similarity of SACs phenomenon in Oe star's HD 34656 spectrum (C IV doublet) with AGNs PG 1254+047 spectrum (Ly $\alpha$  and Si IV and C IV doublets).

Absorption may also appear in low ionization components and transitions of Mg II and sometimes C II, Al II, Al III and C III are present. QSOs with such spectra are called Low ionization BALQSOs (LoBALQSOs), which are defined by the presence of the MgII  $\lambda\lambda$  2798 absorption troughs in addition to the high

ionization ones (Weymann et al. 1991; Voit, Weymann & Korista 1993). The last category includes the so-called FeLoBALs (Hazard et al. 1987), which, in addition to the above mentioned transitions, show broad absorption troughs in lowly ionized iron (e.g. Fe II, Fe III).

Weymann et al. (1991) analyzed a large sample of BALQSOs and defined BALQSOs as quasars exhibiting C IV absorption troughs broader than 2,000 km/s and at least 10% below the continuum at maximum depth. This minimum trough width was defined in order to avoid contamination by noise, but also to reject multiple overlapping intervening systems. A representative line width is  $\sim 10,000$  km/s, although there is considerable diversity among BAL profiles. All BAL identifications are unambiguous since the velocity widths are greater than 2,000 km/s (Brotherton et al. 1998). Velocity widths  $\geq 3,000$  km/s and blue shifted velocities  $\geq 5,000$  km/s are usually considered minimum requirements for classification as a BAL.

The structure of the absorption troughs ranges from apparently very smooth (P-Cygni like) troughs to multiple troughs and/or complexes of many individual absorption lines (Turnshek et al. 1984). In most cases, the observed features have P-Cygni profiles, but sometimes the absorption features appear detached from the emission line by as much as 3,000 km/s. Some BALs have several distinct absorption troughs, while others are strictly “detached” from the emission lines, such that the absorption appears only at blueshifts exceeding several thousand km/s. Multiple troughs are said to be present when several discrete complexes or troughs of absorption exist, separated by several thousand km/s. The existence of multiple troughs is significant because they can impose constraints on model geometry (Turnshek 1986).

BALs clearly identify high velocity outflows (or inflows if the BAL troughs are redshifted with respect to the corresponding emission line) launched from a rotating accretion disc that surrounds and feeds the central black hole. The properties of the BAL material in phase space are uncertain. The properties of BAL material in phase space are uncertain. One opinion is that BALs are the product of a smooth continuous flow (e.g. Scargle et al. 1970, Murray et al. 1995) with the intensity depending on optical depth effects (complete source coverage). On the other hand, it is believed that BALs are due to a flow of many individual substructures in the wind called density enhancements or clumps or clouds, indicating that accretion disc outflows are clumpy (e.g. McKee & Tarter 1975; Turnshek 1984; Lyratzi et al. 2009, 2010, 2011; Hamann et al. 2013; Takeuchi et al. 2013; Misawa et al. 2014; Stathopoulos et al. 2015; Matthews et al. 2016).

According to the second point of view, the broad and complex absorption profiles can be interpreted as the synthesis of a series of absorption components. Sako et al. (2001) state that an important point to note is that the observed velocity widths may as well be due to a superposition of multiple, discrete absorption components each of which are optically thin, and are unresolved with

the RGS. Such features have been observed in UV absorption line spectra of many Seyfert 1 galaxies (Crenshaw et al. 1999, and references therein), some of which (e.g. Mrk 509) show as many as 7 distinct, kinematic components (Kriss et al. 2000). The broad and complex profiles can be interpreted as the synthesis of a series of absorption components. If the latter holds then it implies the existence of independent absorbing regions that cover the continuum and/or emission line region along our line of sight. These absorbing regions can be over densities or density enhancements embedded in a wind produced by an accretion disc.

Recent theoretical and observational evidence point toward a scenario, in which broad absorption lines are the product of clouds or clumps. Takeuchi, Ohsuga & Mineshige (2013), performing global radiation-MHD simulations of supercritical accretion flows onto black holes, found that the outflows associated with supercritical (or super Eddington) accretion flows have a clumpy structure above heights of  $\sim 250 r_s$  (with  $r_s$  being the Schwarzschild radius). The typical clump size is  $\sim 10 r_s$ , which corresponds to about one optical depth, and their shapes are slightly elongated along the outflow direction. They also found that the most plausible cause of clump formation is the Rayleigh-Taylor instability, since the clumpy structure appears in the layer where the upward radiation is superior in force to the downward gravity. Furthermore, a radiation-hydrodynamic instability may also help to form clumps of one optical depth.

Proga et al. (2014) studied the irradiation of clouds by means of numerical, two-dimensional, time-dependent radiation hydrodynamic simulations. They found that even relatively dense clouds that are radiatively heated (i.e., with significant absorption opacity) do not move as a whole; instead, they undergo very rapid and major evolution in shape, size, and physical properties. In particular, the cloud and its remnants become optically thin in less than 1 sound-crossing time and before they can travel a significant distance (a few initial-cloud radii). They also found that a cloud can be accelerated as a whole under quite extreme conditions, i.e., the opacity must be dominated by scattering. However, the acceleration due to the radiation force is relatively small, and unless the cloud is optically thin, it quickly undergoes changes in size and shape.

Misawa et al. (2014) by observing multiple sight lines with the aid of strong gravitational lensing managed to resolve the clumpy structure of the outflow winds in the quasar J1029 +2623. Through their observations they rejected the hypothesis of a smooth homogeneous outflow and concluded to complex small structures inside the outflow from the galactic nucleus. They proposed two different structures for the clumpy outflow: (a) small gas clouds close to the flux source and (b) filamentary (or sheet-like) structure made of multiple clumpy gas clouds.

Proga & Waters (2015) found that optically thin clouds can survive long enough to be accelerated to relatively high velocities and travel a significant distance of many cloud sizes, in contrast to investigations exploring pre-existing optically thick clouds (Proga et al 2014 and references therein).

Recent 2D simulations by Waters & Proga (2016) reveal that the long term evolution of a two-phase medium (hypothetical cloud confining medium proposed by Mathews (1974) and studied extensively by Krolik, McKee & Tarter (1981) - the main idea is of two distinct components, in pressure equilibrium but very different temperature, both heated by the same central source. The gas exposed to the radiation field of a quasar must be in one of two forms: photoionized gas at  $\sim 10^4$  K, which produces optical and UV emission lines, or hot gas at  $T \sim 10^8$  K. The hot phase gas produces the required confinement and the long life of line emitting clouds) in the Broad Line Region (BLR) is a highly turbulent flow that is conducive to continuous cloud production. They also found that cloud production can be maintained because the turbulence supplies perturbations that continually trigger the thermal instability.

Stathopoulos et al. (2017) using the model of Danezis et al. (2003, 2007) as well as Lyrtzi et al. (2007) and the fitting criteria and physical model proposed by Stathopoulos et al. (2015) decomposed the broad absorption troughs of two BALQSOs into the individual components they consist of. They showed that BAL troughs are the product of structures in the wind we call “clouds” and not the product of a smooth continuous flow. They concluded that the “cloud” scenario seems a more plausible explanation for the formation of BAL troughs than the smooth continuous flow interpretation.

Danezis et al. (2007b) noticed that BALs present similar structure to that of the DACs that we can detect in the UV spectra of Hot Emission Stars, Cataclysmic Variables and Wolf Rayet Stars. For this reason they proposed the use of GR model in order to analyze and study BALs. GR model was previously used successfully in analyzing DACs and SACs which appear in the spectra of hot stars.

From the study of BALs a series of questions emerged:

- Can BALs be simulated and analyzed taking into account their complex structure and large widths?
- How can Si IV and C IV BALs be analyzed?
- Accepting the point of view that BALs are the synthesis of a series of spectral line components, is there a way to study not only the whole profile but the profiles of each individual component (line function of each individual absorber in the line of sight)?
- Which is the interpolation polynomial that describes the whole BAL profile?
- In the case of multiple BAL which is the interpolation polynomial that describes the whole absorbing region?
- Can the two members of the resonance doublets, Si IV and C IV, be studied independently? Until now the doublets the resonance doublets (f. e C IV and Si IV) are considered one spectral line.

The ability of GR model to analyze BAL profiles was successfully tested and demonstrated by Stathopoulos et al. (2015). The researchers used GR model in order to analyze the C IV and Si IV resonance lines in the UV spectra of 2 BALQSOs (J01225+1339 and J02287+0002) and proposed a series of criteria which uniquely determine the following:

1. The number of components that construct BALs and
2. The value of the physical parameters (such radial velocities, optical depth, column density, random velocity of the ions, the FWHM, equivalent widths) of the absorbing regions that produce the components of every BAL.

## Our theoretical ad hoc proposed models for DAC/SAC and BAL Regions

Based on the previous arguments concerning the winds of hot stars and quasars, we conclude that the winds of these astronomical objects are far from being smooth. In fact the winds are turbulent and unstable against the radiatively driven instabilities. The instabilities lead to the formation of inhomogeneities and density enhancements referred to as clumps or clouds. We assume that the density of the plasma between these clumps is very low compared to the density of the clumps and as a result we considered it negligible while constructing the mathematical model.

The broad absorption troughs of hot stars and BALQSOs are the product of individual components created by density enhancements in the line of sight towards the observer. Because these components are broad and close in velocity space, they overlap producing the observed smooth profiles which were previously attributed to a smooth continuous flow. The complete picture of the wind structure, in hot stars and BALQSOs, as we consider it is provided below.

### Proposed physical model for DAC Regions

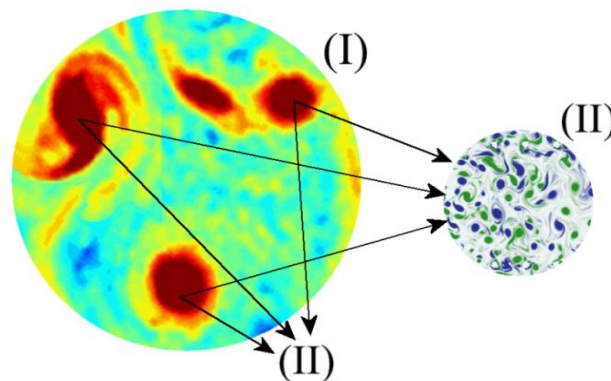


Figure 7. Density regions (I) that form the Discrete Absorption Components (DACs), hence called DAC regions and density regions that form the Satellite Absorption Components (SACs), hence called SAC regions (II).

- The Discrete Absorption Components region (DAC region) (regions I, Fig. 6) consists of independent absorption regions, called SACs regions (regions II, Fig. 6) (Danezis et al. 2003, 2007; Lyratzi et al. 2007).
- The broad profiles of DACs are due to the synthesis of SACs.
- The SAC regions (regions II, Fig. 6) are density enhancements in turbulent flow.
- Due to the turbulent flow, SAC regions rotate with significant velocities.
- The broad profiles of SACs are due to both the self-rotation of the SACs region and the random motion of the matter in these regions.
- The spectral line that corresponds to the SACs are the ones we fit.

**Proposed physical model for the BAL Region (Stathopoulos et al. (2015)).**

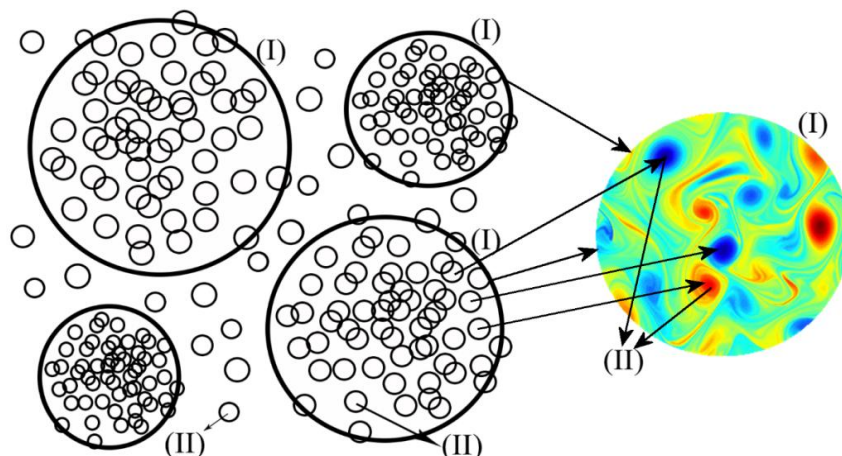


Figure 8. Clouds (I) that form the Broad Absorption Line Regions (BALRs) and cludlets or cloud elements (II) that form the clouds.

- The Broad Absorption Line Region (BALR) consists of independent absorption regions, called clouds (regions I).
- Clouds (regions I) are clusters of cludlets (cloud elements-regions II) in turbulent flow. Cludlets can be thought as density enhancements (clumps) in a continuous medium (Bottorff & Ferland, 2001).
- Each cludlet produces an absorption line, the width of which depends on thermal and microturbulent motions of ions inside the cludlet. The synthesis of all these cludlet lines that are very close in velocity space and overlap, produce a broad component corresponding to a cloud.
- The broad profiles of BALs are due to the synthesis of absorption lines that arise from the clouds.

- The absorption line of each cloud is quite broad, as it is the synthesis of the lines created from the cloudlets that form the cloud. The spectral line that corresponds to the clouds is the ones we fit.

## **The proposed mathematical model (GR model)**

The complex absorption profiles of DACs and BALs raise a series of questions:

- Can DACs and BALs be simulated and analyzed taking into account their complex structure and large widths?
- How can Si IV and C IV DACs and BALs be analyzed?
- Accepting the point of view that DACs and BALs are the synthesis of a series of components, is there a way to study not only the whole profile but the profiles of each individual component (line function of each individual absorber in the line of sight)?
- Which is the interpolation polynomial that describes the whole absorption profile?
- In the case of multiple BALs which is the interpolation polynomial that describes the whole absorbing region?
- Can the two members of the resonance doublets (e.g. Si IV and C IV) be studied independently?
- Until now, in the case of BALs, the resonance doublets of C IV and Si IV were studied as a single line.

In order to answer in this set of questions the “Astrophysical Team” of National and Kapodistrian University of Athens created the GR model (Danezis et al. 2003) which incorporates all the previously mentioned characteristics.

In order to apply GR model to the spectra of all the previously mentioned astronomical objects it was crucial to develop software that can perform simulations and calculations based on GR model.

At this point it is clear that we need to create a software capable, not only to run GR model but to help accelerate complex mathematical precision checks and confirm the uniqueness of the calculated physical parameters.

## **Some important information about GR model**

As we have already mentioned, in order to accept, even theoretically, all the above, we had to construct a mathematical model which would include all the above concepts. This means that by solving the radiation transfer equation for a complex plasma region consisting of independent absorbing and emitting regions, we should calculate the line function, able to reproduce theoretically the observed spectral line profiles.

The term line function corresponds to the function that relates the intensity with the wavelength. This function includes as parameters the physical conditions of the regions that produce the spectral line profile. By giving values

to these parameters, under specific constraints, we try to achieve the best fit of the observed lines profiles.

If we accomplish the best fit, we accept that the theoretical values of the physical parameters are the ones that describe the physical conditions of the regions that produce the line profiles. The problems encountered in the calculation of the line function are the following: A line function able to reproduce theoretically any spectral line of any ion should include all atomic parameters. As a result the line function would be very complex. Also, if we wanted a time dependent line function, we should include time as a parameter. The existence of so many parameters would make the solution of the radiation transfer equation extremely difficult.

In order to overcome some of these difficulties we considered that the line function it not time dependent. The reason for doing so is that as our purpose was to describe the structure of the regions where the SACs are created at a specific moment in time i.e. when the spectrum was taken. In order to study the time-variation of the calculated physical parameters, we should study many spectra of the same star, taken at different periods.

Additionally, we needed a line function with which we could study a specific spectral line of a specific ion, in which case the atomic parameters are constant. In this way, we were able to solve the radiation transfer equations and to find the correct group of parameters that give the best fit of the observed spectral line.

We assume that in the stellar atmosphere the radiation passes through a number of successive independent absorbing and/or emitting density regions of matter until it reaches at the observer.

## **The problem of uniqueness (Stathopoulos et al. 2015)**

The major problem of multicomponent fits is that the best-fit solution is not unique and is depended upon initial parameter guess. So in order to find a final solution, which is unique, and independent of initial parameter/guess we fit simultaneously Si IV and C IV doublets with parameters tied. We assume that both Si IV and C IV follow the same kinematic structure. So Stathopoulos et al. (2015) proposed the following criteria:

### **1. Criteria between the components of a resonance doublet**

(C IV  $\lambda\lambda$  1548.187, 1550.772 Å and Si IV  $\lambda\lambda$  1393.755, 1402.77 Å)

(a) The number of blue and red components of a doublet must be exactly the same. This means that to each component of the 1548.187 Å C IV line corresponds a component of the 1550.772 Å C IV line. The same applies to the Si IV doublet.

(b) Each C IV 1548.187 Å component at a specific velocity shift has its corresponding C IV 1550.772 Å component at the same velocity shift. The same applies to the Si IV doublet. However, we require that the difference in velocities

at line center must not differ from the expected doublet separation by more than one (or two velocity bins depending on how the spectra are binned in velocity space) velocity bin.

(c) The C IV 1548.187 Å component and C IV 1550.772 Å component at the same velocity shift must have the same width. The same applies to the Si IV doublet. The components' FWHM cannot be smaller than the spectrograph's FWHM, which sets an upper limit on the number of components required to achieve the best fit.

(d) For emission lines, the ratio of optical depths between the blue and the red component is  $\tau_b/\tau_r = 2$ , as dictated by atomic physics. For absorption lines this ratio is free to vary  $1:1 \leq \tau_b/\tau_r \leq 2:1$ .

## **2. Criteria between C IV and Si IV components at the same outflow velocity from the corresponding emission redshift.**

(a) Both C IV and Si IV doublets consist of the same number of components.

(b) Each C IV 1548.187 Å (blue) component at a specific velocity shift has its corresponding Si IV 1393.755 Å (blue) component at the same velocity shift. The same applies between the C IV 1550.772 Å (red) components and the Si IV 1402.77 Å (red) components. In practice, Si IV absorption components are shallower than the ones appearing in C IV. So, there is the possibility that a very shallow C IV component has the corresponding Si IV at the same outflow velocity which possibly is not detectable.

(c)  $\tau_b/\tau_r$ (C IV) at a specific velocity shift must be the same as  $\tau_b/\tau_r$  (Si IV) at the same velocity shift. This criterion is applied under the assumption that both doublets (Si IV and C IV) at the same velocity offset are formed in the same outflow and that the physical conditions do not change significantly as a function of velocity.

### Remarks

- We point out that the fitting code is forced to fulfill all the criteria mentioned above. So these criteria are in fact the constraints that are followed during the fitting process and they are not set in order to cross check our results in the end.
- Criterion 2(c) is the only one that can be relaxed during the fitting process. In fact the ratios  $\tau_b/\tau_r$ (C IV) and  $\tau_b/\tau_r$  (Si IV) can be different in the case that C IV and Si IV absorbing systems in the line of sight have different covering fractions, a fact which is pretty usual in the case of BALQSOs.

## The line function and the interpolation polynomial (Danezis et al. 2003)

We assume that we have radiation of intensity  $I_\lambda$  passing through an area of gaseous material of constant density  $\rho$ , thickness  $ds$  and absorption coefficient  $k_\lambda$ . The effect of the shell on the radiation intensity is given by:

$$dI_\lambda = -k_\lambda I_\lambda \rho ds$$

For a density region of total thickness  $s$  and an initial radiation intensity of  $I_{\lambda_0}$  the effect will be:

$$I_\lambda = I_{\lambda_0} \exp(-\tau) \quad (1)$$

where

$$\tau = \int_0^s k_\lambda \rho ds$$

Now consider this radiation intensity passing through a second shell, of density  $\rho_b$ , thickness  $s_b$  and absorption coefficient  $k_{\lambda_b}$ . The radiation intensity exiting this second shell will be:

$$I_{\lambda_b} = I_\lambda \exp(-\tau_b)$$

where:

$$\tau_b = \int_0^{s_b} k_{\lambda_b} \rho_b ds$$

Substituting (1) for  $I_\lambda$  yields:

$$I_{\lambda_b} = I_{\lambda_0} \exp(-\tau) \exp(-\tau_b)$$

Generalising for  $i$  absorbing density regions, the final exiting radiation will be:

$$I_{\lambda_i} = I_{\lambda_0} \prod_i \exp(-\tau_i) \quad (2)$$

Consider now a shell that both absorbs and emits (henceforth called a "mixed" region), with  $k_\lambda$  and  $j_\lambda$  being the respective coefficients. Its effect on the radiation intensity  $I_{\lambda_i}$  will be:

$$dI_{\lambda_i} = -k_\lambda I_{\lambda_i} \rho ds + j_\lambda \rho ds$$

Thus, the total effect of such a shell of thickness  $S_e$ , and density  $\rho_e$  on radiation flow of intensity  $I_{\lambda_i}$  will be:

$$I_{\lambda_e} = I_{\lambda_i} \exp(-\tau_e) + \int_0^{\tau_e} \frac{j_{\lambda_e}}{k_{\lambda_e}} e^{-\tau_e} d\tau$$

where  $j_{\lambda_e}/k_{\lambda_e}$  is the source function  $S_{\lambda_e}$  and

$$\tau_e = \int_0^{s_e} k_{\lambda_e} \rho_e ds$$

At the moment when the spectrum is taken, each emission line, with a given wavelength  $\lambda$ , is created in a specific region of the stellar atmosphere with a given value for  $S_{\lambda_e}$ , that is  $S_{\lambda_e} = const$ . So:

$$I_{\lambda_e} = I_{\lambda_i} \exp(-\tau_e) + S_{\lambda_e} (1 - \exp(-\tau_e)) \quad (3)$$

Now consider that an outer density region of general absorption follows the mixed shell. Its effect on the radiation intensity will be:

$$I_{\lambda_{final}} = I_{\lambda_e} \exp(-\tau_g)$$

in which we replace  $I_{\lambda_e}$  by the radiation intensity exiting the mixed shell, given by equation (3). Thus:

$$I_{\lambda_{final}} = \left[ I_{\lambda_0} \prod_i \exp(-\tau_i) \exp(-\tau_e) + S_{\lambda_e} (1 - \exp(-\tau_e)) \right] \exp(-\tau_g)$$

If we consider the absorption of the mixed region as an independent absorption, we can include it to the product  $\prod_i \exp(-\tau_i)$  and have:

$$I_{\lambda_{final}} = \left[ I_{\lambda_0} \prod_i \exp(-\tau_i) + S_{\lambda_e} (1 - \exp(-\tau_e)) \right] \exp(-\tau_g)$$

Let us consider the parameters  $\tau_i$ ,  $\tau_e$ ,  $\tau_g$ . As stated above, each  $\tau$  is given by:

$$\tau = \int_0^s k_{\lambda} \rho ds$$

We substitute for  $k_{\lambda_i}$ ,  $k_{\lambda_e}$ ,  $k_{\lambda_g}$  the product of two functions:

1. Omega ( $\Omega$ ) is an expression of  $k_{\lambda}$  and has the same units as  $k_{\lambda}$ .
2.  $L_i, L_e, L_g$  are the distribution functions of  $k_{\lambda_i}, k_{\lambda_e}, k_{\lambda_g}$  respectively. Each L depends on the physical conditions of the density region, which forms the spectral line.
- 3.

That is:

$$\tau = L \int_0^s \Omega \rho ds$$

We set:

$$\xi = \int_0^s \Omega \rho ds$$

meaning that  $\xi$  is an expression of  $\tau$ .

The resulting, final form of the radiation flux function is:

$$I_{\lambda_{final}} = \left[ I_0(\lambda) \prod_i \exp(-L_i \xi_i) + S_{\lambda_e} (1 - \exp(-L_e \xi_e)) \right] \exp(-L_g \xi_g)$$

A similar expression applies to the radiation flux:

$$F_{\lambda_{final}} = [F_0(\lambda) \prod_i \exp(-L_i \xi_i) + S_{\lambda_e} (1 - \exp(-L_e \xi_e))] \exp(-L_g \xi_g) \quad (4)$$

where

i: is the number of absorbing density regions that cover the continuum (fully or partially), in the line of sight,

j: is the number of emitting density regions in the line of sight,

g: is the number of additional absorbing density regions that may cover the i absorbing density regions as well as the j emitting density regions,

$I_{\lambda_0}$ : is the initial radiation intensity

$\exp\{-L_i \xi_i\}$ : is the line function of the absorption line i. This means the line function of every one of the components that construct one BAL or DAC

$\prod_i \exp\{-L_i \xi_i\}$ : is the factor that describes the synthesis of absorption lines produced by i density regions. This means that is the interpolation polynomial that can fit every one of DAC or BAL.

$S_{\lambda_{ej}} (1 - \exp\{-L_{ej} \xi_{ej}\})$ : is the line function of the emission line j.

$\sum_j S_{\lambda_{ej}} (1 - \exp\{-L_{ej} \xi_{ej}\})$ : is the factor that describes the summation of emission lines produced by j density regions. This means that is interpolation polynomial that can fit every one of the Broad Emission lines in the case of Quasars or Hot emission stars

$\prod_g \exp\{-L_g \xi_g\}$ : is the factor that describes absorbing density regions that may obscure both the i absorbing as well as the j emitting density regions.

$L_i, L_{ej}, L_g$ : are the distribution functions of the absorption coefficients

$k_{\lambda i}, k_{\lambda ej}, k_{\lambda g}$ ,

$k_{\lambda i}$ : is the absorption coefficient of the i<sup>th</sup> density region in the line of sight,

$k_{\lambda ej}$ : is the emitting coefficient of the  $j$ th density region in the line of sight,  
 $k_{\lambda g}$ : is the absorption coefficient of the additional absorbing density regions that may cover the  $i$  and  $j$  density regions in the line of sight,  
 $\xi$ : is the optical depth in the center of the spectral line,  
 $S_{\lambda ej}$ : is the source function that is constant during one observation

Equation (4) gives the function of the complex profile of a spectral line, which presents SACs. This means that the graphical representation of Eq. (4) must reproduce not only the main spectral line, but its SACs as well. As we can deduce from the above, the calculation of  $F_{\lambda_{final}}$  does not depend on the geometry of the absorbing or emitting independent density layers of matter.

The decision on the geometry is essential for the calculation of the parameters  $L_i$ . This means that by deciding on a different geometry we conclude to a different analytical form of  $L_i$ , and thus to a different shape of the profile of the spectral line, presenting SACs, that we study.

In order to decide on the appropriate geometry we took into consideration the following important facts:

1. The spectral line's profile was reproduced in the best way when we supposed spherical symmetry for the independent density regions. Such symmetry has been proposed by many researchers (Lamers et al. 1982, Bates & Gilheany 1990, Gilheany et al. 1990, Waldron et al. 1992, Rivinius et al. 1997, Cidale 1998, Markova 2000).
2. However, the independent regions of matter, where a spectral line and its SACs were born, could lie either close to the star, as in the case of the photospheric components of the H $\alpha$  line in Be stars (Andrillat & Fehrenbach 1982, Andrillat 1983), in which case spherical symmetry around the star is justified, or at a greater distance from the star, where the spherical symmetry around the star cannot be justified.

These thoughts lead us to the conclusions that:

1. In the case of independent density regions of matter that lie close to the star we could suppose the existence of a classical spherical symmetry around the star.
2. In the case of greater distance from the photosphere, we could suppose the existence of independent density regions of matter such as clumps, (Cranmer & Owocki 1996) which are outwards moving inhomogeneities (Rivinius et al. 1997), spiral streams (Fullerton et al. 1997, Cranmer et al. 2000, Markova 2000) or CIRs, which may result from non-radial pulsations, magnetic fields or the star's rotation (Mullan 1984a,b, 1986, Prinja & Howarth 1988, Kaper et al. 1996, 1997, 1999) and are able to make structures that cover a substantial portion of the stellar disk (Cranmer & Owocki 1996, Kaper et al. 1996, 1997, 1999). These regions, though they are not necessarily spherically symmetric, they form spectral line profiles which are identical to those deriving from a spherically symmetric structure. This means that these line profiles present the same values

for  $V_{\text{rot}}$ ,  $V_{\text{rad}}$  and  $\xi$  as the ones deriving from a classical spherical symmetry. In such a case, though the density regions are not necessarily spherically symmetric, through their effects on the lines' profiles, they appear to the observer as spherically symmetric structures around their own center. This means that in both cases, where either the symmetry is spherical or it appears as spherical through its effects on the lines' profile, the calculation of  $L_i$ , is justifiably based on the supposition of spherical symmetry.

The above mentioned thoughts led us to suppose spherical symmetry (or apparent spherical symmetry) for the density regions where the main spectral line as well as its SACs are born, in order to calculate the parameters  $L_i$ .

### The mathematical expressions of L

$\exp(-L_i \xi_i)$  and  $S_{\lambda_{ej}}(1 - \exp(-L_i \xi_i))$  are the distribution functions of the absorption and the emission satellite component, respectively. The factor L must include the geometry and all the physical conditions of the region that produces the spectral line. These physical conditions indicate the exact distribution that we must use. This means that if we choose the right physical conditions in the calculations of the factor L, the functions  $\exp(-L_i \xi_i)$  and  $S_{\lambda_{ej}}(1 - \exp(-L_i \xi_i))$  can have the form of a different distribution function, i.e. Gauss if the line broadening is only due to the random motions, Lorentz if line broadening is only due to the pressure or Voigt if the line broadening is due to random motions and pressure.

In GR model, we do not use the pure mathematical distributions that do not include any physical parameter, but the above mentioned physical expression of these distributions.

1. If  $L_\lambda$  has the form

$$L_\lambda = \xi e^{-\frac{(\lambda - \lambda_0)^2}{2\sigma^2}}, \text{ where } \xi \text{ is the height of the spectral line's component and}$$

$$\xi = \frac{1}{\sqrt{2\pi}\sigma^2}$$

the line function  $\exp(-L_i \xi_i)$  that describes an absorption line, has the form of a Gauss distribution.

2. If  $L_\lambda$  has the form

$$L_\lambda = \frac{\xi}{1 + \left(\frac{\lambda - \lambda_0}{\gamma}\right)^2}, \text{ where } \xi \text{ is the height of the spectral line's component, the}$$

line function  $\exp(-L_i \xi_i)$  that describes an absorption line, has the form of a Lorentz distribution.

3. If  $L_\lambda$  has the form

$$L_\lambda = \int_{-\infty}^{+\infty} \frac{e^{-\frac{(\lambda' - \lambda_0)^2}{2\sigma^2}}}{1 + \frac{(\lambda - \lambda')^2}{\gamma^2}} d\lambda'$$

the line function  $\exp(-L_i \xi_i)$  that describes an absorption line, has the form of a Voigt distribution.

Similarly, if we put the above expressions of  $L_\lambda$  (cases 1, 2, 3) in the emission line function  $S_{\lambda_{ej}}(1 - \exp(-L_{ej} \xi_{ej}))$  it will take the form of a Gauss, Lorentz or Voigt distribution.

### **Constructing two new distribution functions**

Hot emission stars rotate close to break-up velocities, and a mechanism – the so-called e phenomenon – acts in addition to rotation, leading to episodic or continuous mass ejection from the stellar equator. The produced wind is turbulent and unstable against the radiatively driven instabilities. The instabilities lead to the formation of inhomogeneities and density enhancements referred to as clumps or clouds. For these reasons we hypothesized that the absorbing regions that produce DACs and/or SACs rotate around their own centers. As a result, the rotation of the independent absorbing regions plays a crucial role in the broadening of the produced spectral lines. As a result, we had to include the rotation of the density regions, around their own centers, to our model, in order to simulate the observed profiles.

As a first step, Danezis et al. (2003) and Lyratzi et al. 2007 constructed a distribution function  $L$  that considers as the only reason of line broadening the rotation of the regions, that produce the spectral lines, around their own centers. The distribution was called Rotation.

However, in a gas at temperature  $T$ , individual atoms will have random motions away from or towards the observer, leading to red- or blue-wards frequency shifts. Another broadening process is the so called microturbulence for which a gaussian line-of-sight velocity distribution is adopted. As a result the distribution that describes random motions (thermal and non thermal) is Gauss.

In order to include both factors (rotation and random motions) in line broadening Danezis et al. (2007a) combined Rotation distribution and Gauss distribution to create Gauss-Rotation distribution.

### **The rotation distribution function (Lyratzi et al. 2007)**

Let us assume that the main reason of the line broadening is the rotation of the regions that produce each satellite component of the whole observed spectral feature. These rapidly rotating density regions may also present radial motion.

For these reasons we look for another expression of the distribution function of the spectral line's components that has as parameters the rotational and radial velocities of the spherical density regions. For a spherical density region, we make the following assumptions:

1. Thermal and natural broadening of spectral lines are negligible. This means that the whole width of the line is measured as  $V_{rot}$ .
2. None of the phenomena are relativistic.
3. The only effect of a density region's radial movement is a Doppler shift of the spectral lines' centers.
4. Lambert's sinus law stands for each point of the spherical region.
5. The angular velocity of rotation is constant.

In order to calculate the total radiation, we divide the spherical layer in very thin cylindrical surfaces which are vertical to the rotational axis. Lambert's law allows us to consider that the luminosity from each point on the sphere is the same.

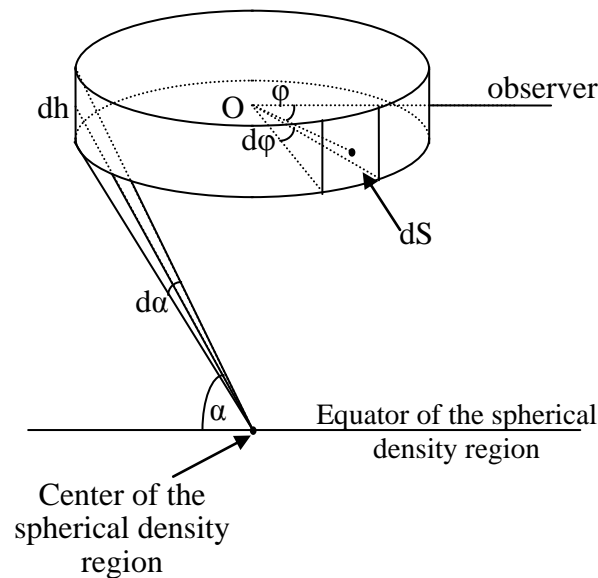


Figure 9. Elementary ring of the spherical density region.

In the above cylindrical surfaces we also consider the surface  $dS$ . According to Lambert's law, when this surface rotates with an angular velocity  $\omega$ , its radiation intensity is:

$$dI(\omega) = Q(\omega) dS \cos\theta \quad (5)$$

where:

$\theta$  is the angle between the vertical on  $dS$  and the line of sight and

$$Q(\omega) = C_1 \frac{\gamma}{(\omega - \omega_k)^2 + \left(\frac{\gamma}{2}\right)^2}$$

where  $C_1$  is a constant and  $\gamma$  is the Lorentz full width at half intensity maximum, which, in the case of the natural broadening, has the value  $\gamma \cong 10^8$  Hz. When the surface  $dS$  does not rotate, the center of the formed spectral line lies on the observed wavelength  $\lambda_0$ , which corresponds to frequency  $\nu_0$ . Thus, we have:

$$\omega_0 = 2\pi\nu_0 = 2\pi \frac{c}{\lambda_0}.$$

When the surface  $dS$  rotates with rotational velocity  $V_{rot}$  the center of the formed line lies on the wavelength  $\lambda_k$  and in this case we have  $\omega_k = \omega_0(1 - z\sin\varphi)$ , where  $z = \frac{V_{rot}}{c}$

We also have  $\cos\theta \cong \cos\alpha \cos\varphi$ . The angles  $\alpha$  and  $\varphi$  are shown in Fig. 9.  $dS$  can be written as  $dS = rdhd\varphi$ , where  $r$  is the radius of the cylinder,  $d\varphi$  is the angle under which we see the basis of  $dS$  and  $dh$  is the height of  $dS$ . Making the above substitutions in Eq. (6) we have:

$$dI(\omega) = \frac{C_1 rdh\gamma \cos\alpha \cos\varphi d\varphi}{[\omega - \omega_0(1 - z\sin\varphi)]^2 + \left(\frac{\gamma}{2}\right)^2}$$

Thus, the radiation intensity of the semi cylinder is

$$I(\omega) = \int_{-\pi/2}^{\pi/2} \frac{C_1 rdh\gamma \cos\alpha \cos\varphi d\varphi}{[\omega - \omega_0(1 - z\sin\varphi)]^2 + \left(\frac{\gamma}{2}\right)^2}$$

or

$$I(\omega) = \frac{4C_1 rdh}{\gamma} \int_{-\pi/2}^{\pi/2} \frac{\cos\alpha d\sin\varphi}{\left[\left(\frac{\omega}{\gamma/2}\right) - \left(\frac{\omega_0}{\gamma/2}\right)(1 - z\sin\varphi)\right]^2 + 1}$$

We set  $\tilde{\omega} = \frac{\omega}{\gamma/2}$ ,  $\tilde{\omega}_0 = \frac{\omega_0}{\gamma/2}$ ,  $x = \sin\varphi$  and we have

$$I(\tilde{\omega}) = \frac{4C_1 r \cos\alpha dh}{\gamma} \int_{-1}^1 \frac{dx}{[\tilde{\omega} - \tilde{\omega}_0(1 - zx)]^2 + 1}$$

We also set  $y = \tilde{\omega} - \tilde{\omega}_0(1 - zx)$  and the above integral becomes

$$I(\tilde{\omega}) = \frac{4C_1 r \cos\alpha dh}{\gamma \tilde{\omega}_0 z} \int_{\tilde{\omega} - \tilde{\omega}_0(1+z)}^{\tilde{\omega} - \tilde{\omega}_0(1-z)} \frac{dy}{y^2 + 1}$$

Finally, we have

$$I(\tilde{\omega}) = \left(\frac{4C_1 r \cos\alpha dh}{\gamma}\right) \left(\frac{\arctan[\tilde{\omega} - \tilde{\omega}_0(1-z)] - \arctan[\tilde{\omega} - \tilde{\omega}_0(1+z)]}{\tilde{\omega}_0 z}\right) \quad (6)$$

The above function describes the radiation intensity of a semi cylinder with radius  $r$  and height  $dh$ .  $d\alpha$  is the observational angle of  $dh$  from the center of the spherical region. This cylinder rotates with a rotational velocity  $z = V_{rot}/c$  and a constant angular velocity  $\tilde{\omega}$ .

We consider the function:

$$P(\tilde{\omega}, z) = \frac{\arctan[\tilde{\omega} - \tilde{\omega}_0(1 - z)] - \arctan[\tilde{\omega} - \tilde{\omega}_0(1 + z)]}{\tilde{\omega}_0 z}$$

We study the limit of this function in the case when the density layer does not rotate, i.e. when  $z \rightarrow 0$ , meaning:

$$\lim_{z \rightarrow 0} P(\tilde{\omega}, z) = \lim_{z \rightarrow 0} \frac{\arctan[\tilde{\omega} - \tilde{\omega}_0(1 - z)] - \arctan[\tilde{\omega} - \tilde{\omega}_0(1 + z)]}{\tilde{\omega}_0 z}$$

We apply the L' Hospital's rule and we get:

$$\lim_{z \rightarrow 0} P(\tilde{\omega}, z) = \lim_{z \rightarrow 0} \frac{\frac{d}{dz} \{\arctan[\tilde{\omega} - \tilde{\omega}_0(1 - z)]\} - \frac{d}{dz} \{\arctan[\tilde{\omega} - \tilde{\omega}_0(1 + z)]\}}{\frac{d}{dz} (\tilde{\omega}_0 z)}$$

$$\begin{aligned} \lim_{z \rightarrow 0} P(\tilde{\omega}, z) &= \lim_{z \rightarrow 0} \left[ \frac{1}{1 + [\tilde{\omega} - \tilde{\omega}_0(1 - z)]^2} + \frac{1}{1 + [\tilde{\omega} - \tilde{\omega}_0(1 + z)]^2} \right] \\ &= \frac{2}{(\tilde{\omega} - \tilde{\omega}_0)^2 + 1} \end{aligned}$$

This form corresponds to the Lorentz's distribution of the natural broadening of the spectral lines. In the case when the rotation broadening  $|\lambda_1 - \lambda_2|$  (or  $|\omega_1 - \omega_2|$ ) is much larger than the natural broadening (the natural broadening of a spectral line is about  $10^{-3} - 10^{-4}$  Å), the above function  $P(\tilde{\omega}, z)$  present the form of a square pulse (see Fig. 10).

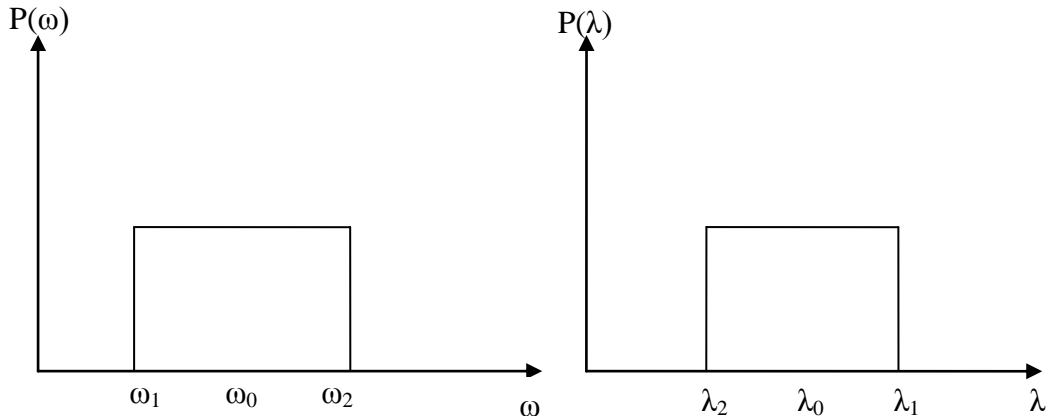


Figure 10. Quadratic pulsation

For each  $\omega$  with  $\omega_1 < \omega < \omega_2$  the relative shift is  $z = \frac{|\Delta\omega|}{\omega_0}$ . For the point  $\omega_1$  we have  $\frac{\omega_0 - \omega_1}{\omega_0} = z$  and so  $\omega_1 = \omega_0(1 - z)$ .

Likewise, for the point  $\omega_2$  we have  $\omega_2 = \omega_0(1 + z)$ . But  $\omega = 2\pi\nu = \frac{2\pi c}{\lambda}$ . Thus,  $\lambda_1 = \frac{\lambda_0}{1-z}$  and  $\lambda_2 = \frac{\lambda_0}{1+z}$  with  $\lambda_1 > \lambda_2$ .

This means that  $\Delta\lambda_{total} \equiv \lambda_1 - \lambda_2 = \frac{2\lambda_0 z}{1-z^2}$  and so

$$\lambda_{\min} \equiv \lambda_2 = \lambda_0 - \frac{\Delta\lambda_{total}}{2} = \lambda_0 - \lambda_0 \frac{z}{1-z^2} \text{ and}$$

$$\lambda_{\max} \equiv \lambda_1 = \lambda_0 + \frac{\Delta\lambda_{total}}{2} = \lambda_0 + \lambda_0 \frac{z}{1-z^2}.$$

We set  $\rho = \lambda_0 \frac{z}{1-z^2}$  and normalize to 1. In this way the function  $P(\tilde{\omega}, z)$  could be approximated with the function  $f(\lambda)$  where:

$$f(\lambda) = \begin{cases} 1 & \text{if } |\lambda - \lambda_0| < \rho \\ 0 & \text{otherwise} \end{cases}$$

Now, we suppose that the spherical density region rotates with equatorial velocity  $z_0 = \frac{V_0}{c}$  (see the Fig 11).

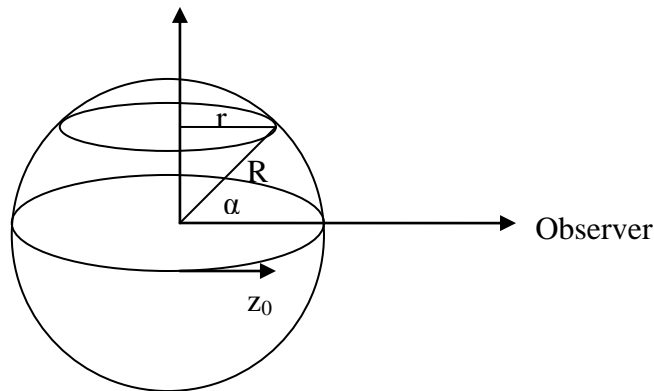


Figure 11. Rotating spherical density region that produces SACs or DACs.

The points of the circle with radius  $r$  rotate with a velocity  $V_{rot}$  and for  $r = R\cos\alpha$  we get

$$V_{rot} = \omega r = \omega R\cos\alpha \stackrel{\omega = \text{const}}{=} \frac{V_0}{R} R\cos\alpha = V_0\cos\alpha \text{ and so } z = z_0\cos\alpha. \text{ We have also } dh = R d\alpha \text{ and Eq. (6) becomes}$$

$$dI(\tilde{\omega}) = \frac{4C_1 R}{\gamma} \cdot \frac{\arctan[\tilde{\omega} - \tilde{\omega}_0(1 - z_0\cos\alpha)] - \arctan[\tilde{\omega} - \tilde{\omega}_0(1 + z_0\cos\alpha)]}{\tilde{\omega}_0 z_0 \cos\alpha}$$

The integral of this equation is

$$I(\tilde{\omega}) = \frac{4C_1 R}{\gamma} \int_{-\pi/2}^{\pi/2} \frac{\arctan[\tilde{\omega} - \tilde{\omega}_0(1 - z_0\cos\alpha)] - \arctan[\tilde{\omega} - \tilde{\omega}_0(1 + z_0\cos\alpha)]}{\tilde{\omega}_0 z_0 \cos\alpha} \cos\alpha d\alpha$$

When we take into account the function  $P(\tilde{\omega}, z)$  the above function becomes

$$I(\tilde{\omega}) = \frac{4C_1R}{\gamma} \int_{-\pi/2}^{\pi/2} P(\tilde{\omega}, z_0 \cos \alpha) \cos \alpha d\alpha$$

We approximate  $P(\tilde{\omega}, z_0 \cos \alpha)$  with  $f(\lambda)$  and we take the integral for the observation angle  $\theta \in [-\theta_0, \theta_0]$  from the equatorial plane.

So we have that

$$I(\tilde{\omega}) \cong I_1 = \frac{4C_1R}{\gamma} \int_{-\theta_0}^{\theta_0} 1 \cdot \cos \theta d\theta.$$

$$I_1 = \frac{4C_1R}{\gamma} \int_{-\theta_0}^{\theta_0} \cos \theta d\theta = \frac{4C_1R}{\gamma} [\sin \theta]_{-\theta_0}^{\theta_0} = \frac{8C_1R}{\gamma} \sin \theta_0.$$

If we normalize to 1, we have

$$I_1 \cong \sin \theta_0 = \sqrt{1 - \cos^2 \theta_0}.$$

For the angle  $\theta_0$  we have

$$|\lambda - \lambda_0| \leq \rho_0 = \frac{\lambda_0 z_0 \cos \theta_0}{1 - z_0^2 \cos^2 \theta_0}.$$

For a wavelength  $\lambda$  or for a shift  $\Delta\lambda = |\lambda - \lambda_0|$  from the center of the spectral line, the absorbing (or emitting) regions are those with angular distance  $\theta$  from the equatorial plane, with  $|\theta| \leq \theta_0$ . For the equatorial plane we have

$$\Delta\lambda = \frac{\lambda_0 z_0 \cos \theta_0}{1 - z_0^2 \cos^2 \theta_0}.$$

From this equation we can calculate the angle  $\theta_0$  as follows:

$$\cos \theta_0 = \frac{-\lambda_0 \pm \sqrt{\lambda_0^2 + 4\Delta\lambda^2}}{2\Delta\lambda z_0}.$$

As  $\theta_0$  is between  $-\pi/2$  and  $\pi/2$  we have  $\cos \theta_0 \geq 0$  and so

$$\cos \theta_0 = \frac{-\lambda_0 + \sqrt{\lambda_0^2 + 4\Delta\lambda^2}}{2\Delta\lambda z_0}.$$

Thus, the distribution function  $I_1$  takes its final form:

$$I_1 = \sqrt{1 - \cos^2 \theta_0} \text{ if } \cos \theta_0 = \frac{-\lambda_0 + \sqrt{\lambda_0^2 + 4\Delta\lambda^2}}{2\Delta\lambda z_0} < 1 \text{ and}$$

$I_1 = 0$ , other wise.

It is obvious that the distribution function  $I_1$  is a function of the wavelength  $\lambda$ . This means that  $I_1 = I_1(\lambda)$ . This distribution function has the same form with the distribution function of the absorption coefficient  $L$  and may replace it (in  $e^{-L\xi}$ ), when the main reason of the line broadening is rotation. We call it Rotation distribution function. The spectral line profile, which is formed by a spherical density region, is reproduced by the function  $\exp(-L\xi)$  by applying the appropriate value of the rotational velocity  $V_{rot}$  (from  $z_0$ ), the radial velocity  $V_{rad}$  (from  $V_{rad}/c = (\lambda_0 - \lambda_{lab})/\lambda_{lab}$ ) and the optical depth  $\xi$  in the center of the line.

### **Including random motion in the calculation of L**

#### **The Gauss-Rotation distribution function (GR distribution function) (Danezis et al. 2007a)**

One of the assumptions, when constructing the Rotation distribution, was that the line width  $\Delta\lambda$  is only due to rotation. This means that the random velocities of the ions in the density region are very low and they do not contribute to line broadening. In a new approach of the problem we also consider the random velocities in the calculation of the distribution function L (Danezis et al. 2007a).

We consider a spherical shell and a point  $A_i$  in its equator. If the laboratory wavelength of a spectral line that arises from  $A_i$  is  $\lambda_0$ , the observed wavelength will be:

$$\lambda_i = \lambda_0 \pm \Delta\lambda_i \text{ and}$$

$$\Delta\lambda_i = \lambda_0 z \sin\varphi, \quad z = V_{rot}/c$$

Where  $V_{rot}$  is the rotational velocity of point  $A_i$ .

This means that

$$\lambda_i = \lambda_0 \pm \lambda_0 z \sin\varphi = \lambda_0(1 \pm z \sin\varphi)$$

$$\text{and if } -\frac{\pi}{2} < \varphi < \frac{\pi}{2}$$

then

$$\lambda_i = \lambda_0(1 - z \sin\varphi)$$

If we assume that the spectral line profile is a Gaussian distribution

$$I(\lambda) = \frac{1}{\sqrt{2\pi}\sigma} e^{-\left(\frac{\lambda-k}{\sigma\sqrt{2}}\right)^2}$$

where  $k$  is the mean value of the distribution and in the case of the line profile it indicates the center of the spectral line that arises from  $A_i$ . This means that:

$$I(\lambda) = \frac{1}{\sigma\sqrt{2\pi}} e^{-\left[\frac{\lambda-\lambda_0(1-z\sin\varphi)}{\sigma\sqrt{2}}\right]^2} = \frac{1}{\sigma\sqrt{2\pi}} e^{-\frac{[\lambda-\lambda_0(1-z\sin\varphi)]^2}{2\sigma^2}}$$

The distribution function for all the semi-equator is:

$$I_1(\lambda) = \int_{-\frac{\pi}{2}}^{\frac{\pi}{2}} \frac{1}{\sqrt{2\pi}\sigma} e^{-\frac{[\lambda-\lambda_0(1-z\sin\varphi)]^2}{2\sigma^2}} \cos\varphi d\varphi$$

If  $\sin\varphi = x$  then  $dx = \cos\varphi d\varphi$  and  $-1 \leq x \leq 1$ , so Eq. (10) takes the form

$$I_1(\lambda) = \int_{-1}^1 \frac{1}{\sigma\sqrt{2\pi}} e^{-\frac{[\lambda-\lambda_0(1-zx)]^2}{2\sigma^2}} dx$$

If we set  $u = \frac{\lambda-\lambda_0(1-zx)}{\sqrt{2}\sigma}$ , we have

$$I_1(\lambda) = \frac{1}{\lambda_0 z \sqrt{\pi}} \int_{\frac{\lambda-\lambda_0(1+z)}{\sigma\sqrt{2}}}^{\frac{\lambda-\lambda_0(1-z)}{\sigma\sqrt{2}}} e^{-u^2} du$$

We consider the function

$$erf(x) = \frac{2}{\pi} \int_0^x e^{-u^2} du.$$

It is the known function which describes the Gaussian error distribution. If we take into account this function,  $I_1(\lambda)$  takes the form

$$I_1(\lambda) = \frac{1}{\lambda_0 z \sqrt{\pi}} \left[ \int_0^{\frac{\lambda-\lambda_0(1-z)}{\sigma\sqrt{2}}} e^{-u^2} du - \int_0^{\frac{\lambda-\lambda_0(1+z)}{\sigma\sqrt{2}}} e^{-u^2} du \right]$$

$$I_1(\lambda) = \frac{1}{\lambda_0 z \sqrt{\pi}} \left[ \frac{\pi}{2} erf\left(\frac{\lambda-\lambda_0(1-z)}{\sigma\sqrt{2}}\right) - \frac{\pi}{2} erf\left(\frac{\lambda-\lambda_0(1+z)}{\sigma\sqrt{2}}\right) \right]$$

Thus, we finally have

$$I_1(\lambda) = \frac{\sqrt{\pi}}{2\lambda_0 z} \left[ erf\left(\frac{\lambda-\lambda_0(1-z)}{\sigma\sqrt{2}}\right) - erf\left(\frac{\lambda-\lambda_0(1+z)}{\sigma\sqrt{2}}\right) \right]$$

and the distribution function from the semi-spherical region is:

$$I_{final}(\lambda) = \frac{\sqrt{\pi}}{2\lambda_0 z} \int_{-\frac{\pi}{2}}^{\frac{\pi}{2}} \left[ erf\left(\frac{\lambda - \lambda_0}{\sigma\sqrt{2}} + \frac{\lambda_0 z}{\sigma\sqrt{2}} \cos\theta\right) - erf\left(\frac{\lambda - \lambda_0}{\sigma\sqrt{2}} - \frac{\lambda_0 z}{\sigma\sqrt{2}} \cos\theta\right) \right] \cos\theta d\theta$$

### **Note**

The error function

$$erf(x) = \frac{2}{\pi} \int_0^x e^{-u^2} du$$

is well defined and is characterized by the following properties:

1.  $erf(-x) = -erf(x)$
2.  $erf(0) = 0$
3.  $erf(+\infty) = 1$  καθώς  $\lim_{x \rightarrow +\infty} erf(x) = 1$
4.  $erf(-1) = -1$
5.  $erf(x) = \frac{2}{\sqrt{\pi}} \left( x - \frac{x^3}{3 \cdot 1!} + \frac{x^5}{5 \cdot 2!} - \frac{x^7}{7 \cdot 3!} + \dots \right)$
6.  $erf(x) = 1 - \frac{e^{-x^2}}{\sqrt{\pi} x} \left( 1 - \frac{1}{2x^2} + \frac{1 \cdot 3}{(2x^2)^2} - \frac{1 \cdot 3 \cdot 5}{(2x^2)^3} + \dots \right)$

As the described distribution combines the random motions of the ions in a density region with the rotation of this region, we refer to it through the designation G (Gauss) R (Rotation). Also, as we constructed the Gauss-Rotation distribution in order to use it in this model, we also applied the same name to our model (GR model).

### **Important Notice**

We remind that Eq. (4) is the interpolation polynomial that describes the whole absorbing region in the case of multiple BALs.

$$F(\lambda)_{final} = \left[ F_0(\lambda) \prod_i \exp\{-L_i \xi_i\} + \sum_j S_{\lambda_{ej}} (1 - \exp\{-L_{ej} \xi_{ej}\}) \right] \prod_g \exp\{-L_g \xi_g\} \quad (4)$$

During the fitting process of a resonance doublet we use Eq. (4) independently for every component. For example in the case of C IV  $\lambda\lambda$  1548.187, 1550.772 Å resonance lines, we apply Eq. (1) twice, once for the 1548.187 Å (blue) and once for the 1550.772 Å (red) component of the doublet. By applying Eq. (4) twice we get two sets of lines. The first one contains all the blue components of C IV doublet while the second one contains all the red components of C IV doublet. Having these two sets of lines we then synthesize them to get the best fit. In the case of absorption lines we use Gauss distribution while in the case of emission lines we use Voigt distribution. We point out that after the continuum fit we fit the broad emission lines (see Fig. 12).

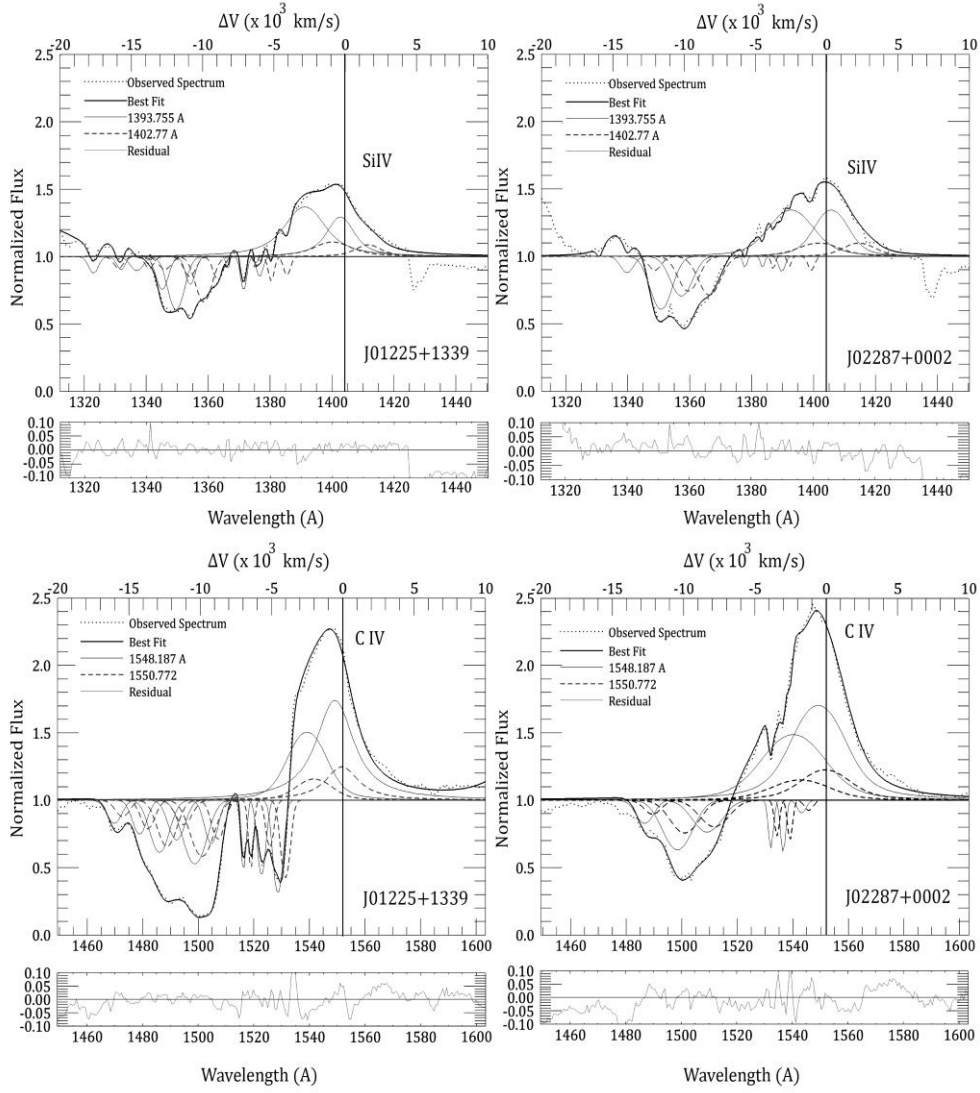


Figure 12. Best fits of the Si IV and C IV spectral regions of J01225+1339 and J02287+0002. The black dotted line denotes the observed spectrum while black, thick solid line corresponds to the best fit. We denote the shorter wavelength member of a doublet with blue thin solid line (blue: 1393.755 Å for Si IV and 1548.187 Å for C IV) while we denote the longer wavelength member of a doublet with the red dashed line (red: 1402.77 Å for Si IV and 1550.772 Å for C IV). The zero velocity corresponds to the longer wavelength member of a doublet. Below each fit we present a panel with the residual, which appears in green thin line. Furthermore, the reduced  $\chi^2$  is given for every fit. Note that the value of the reduced  $\chi^2$  serves only as a qualitative measure of the fit and should not be interpreted as indicating the probability of the fit (Stathopoulos et al. 2015)

## Parameter Calculation

### Random velocities of ions ( $V_{random}$ ) in the case of Gauss

We have:

$$\frac{V_{random}}{c} = \frac{\Delta\lambda_{halfwidth}}{\lambda_0}$$

where  $\Delta\lambda_{halfwidth} = |\lambda - \lambda_0|$  at half of the depth of the spectral line.

The Gaussian distribution is given by

$$L = e^{-\frac{\Delta\lambda_{half\ width}}{2\sigma^2}}$$

At the half of the depth of the spectral line we have  $L=1/2$ . Thus, the previous relation has the form:

$$L = e^{-\frac{\Delta\lambda_{half\ width}}{2\sigma^2}}$$

Then:

$$\Delta\lambda_{half\ width} = \sigma\sqrt{2\ln 2}$$

So, for  $V_{random}$  we get

$$V_{random} = \frac{\sigma c\sqrt{2\ln 2}}{\lambda_0}$$

## Calculation of the FWHM

### Absorption

The radiation intensity for a specific density region is generally given by the function

$$I = I_0 e^{-L\xi}$$

For  $L=0$ ,  $I=I_0$  (continuum).

For  $L=1$ ,  $I=I_0 e^{-\xi}$

Thus, the depth of the line is  $I_0 - I_0 e^{-\xi} = I_0(1 - e^{-\xi})$

The half depth of the line is  $\frac{1}{2}I_0(1 - e^{-\xi})$

The half depth of the line corresponds to a specific value of  $L$ . We call this value (as above)  $L_{halfwidth}$ .

In this case the depth of the line is  $I_0(1 - e^{-\xi L_{halfwidth}})$

Obviously, it must be  $I_0(1 - e^{-\xi L_{halfwidth}}) = \frac{1}{2}I_0(1 - e^{-\xi})$

$$\text{So } L_{halfwidth} = \frac{\ln 2 - \ln(1 + e^{-\xi})}{\xi}$$

For the Gaussian distribution we have  $L = e^{-\frac{(\lambda - \lambda_0)^2}{2\sigma^2}}$

Thus, for  $L = L_{halfwidth}$  we get  $L_{halfwidth} = e^{-\frac{(\frac{FWHM}{2})^2}{2\sigma^2}}$

$$\text{So } FWHM = 2\sigma\sqrt{-2\ln L_{halfwidth}}$$

It is obvious that  $\ln L_{halfwidth} < 0$  because  $0 < L_{halfwidth} < 1$ . So, the above function gives a real number.

### Emission

In the case of emission the radiation intensity is  $I = S(1 - e^{-L\xi})$

For  $L=1$  we have  $L=S(1-e^{-\xi})$ .

For  $L=0$  we have  $L=0$  (continuum).

Thus, the height of the emission line is  $S(1 - e^{-\xi})$

At the half of the height we have  $\frac{1}{2}S(1 - e^{-\xi})$

The half of the height corresponds to a specific value of  $L$ . We call this value  $L_{halfwidth}$ . In this value the radiation intensity is  $S(1 - e^{-\xi L_{halfwidth}})$

It must be  $\frac{1}{2}S(1 - e^{-\xi}) = S(1 - e^{-\xi L_{halfwidth}})$

$$\text{So } L_{halfwidth} = \frac{\ln 2 - \ln(1 + e^{-\xi})}{\xi}$$

As in the case of the absorption we get  $FWHM = 2\sigma\sqrt{-2\ln L_{halfwidth}}$

As in the case of the absorption we take

$$FWHM = 2\sigma\sqrt{-2\ln L_{halfwidth}}$$

### Rotation distribution

#### Absorption

At first, we calculate the  $L_{halfwidth}$  as in the case of the Gaussian distribution.

$$L_{halfwidth} = \frac{\ln 2 - \ln(1 + e^{-\xi})}{\xi}$$

For the Rotation distribution we generally have

$$L = \sqrt{1 - \frac{(\lambda - \lambda_0)^2}{\lambda_0^2 z^2}}$$

where  $z = \frac{V_{rot}}{c}$ .

For  $L = L_{halfwidth}$  we get

$$L_{halfwidth} = \sqrt{1 - \frac{(\frac{FWHM}{2})^2}{\lambda_0^2 z^2}}$$

So we get

$$FWHM = \frac{2\lambda_0 z}{\xi} \sqrt{\xi^2 - [\ln 2 - \ln(1 + e^{-\xi})]^2}$$

This expression is a real number because  $\xi > 0$ .

### Emission

As in the case of emission in the Gaussian distribution we calculate the  $L_{halfwidth}$  and then we have

$$FWHM = \frac{2\lambda_0 z}{\xi} \sqrt{\xi^2 - [\ln 2 - \ln(1 + e^{-\xi})]^2}$$

### Gauss-Rotation distribution

In this case we calculate the FWHM using an arithmetical method. The spectral line profile is generally described by the function

$$F(L(\lambda)) = e^{-L(\lambda)\xi}$$

In the case of the Gauss- Rotation (GR) distribution, the spectral line profile is given by

$$F(L_{GR}(\lambda)) = e^{-L_{GR}(\lambda)\xi}$$

where  $L_{GR}$  is a combination (composition) of Gauss and Rotation distributions, with

$$L_G = e^{-\frac{(\lambda - \lambda_0)^2}{2\sigma^2}}$$

and

$$L_R = \sqrt{1 - \frac{(\lambda - \lambda_0)^2}{\lambda_0^2 z^2}}$$

for the Gauss and the Rotation distribution respectively.

We calculate  $\lambda_{halfwidth}$  using arithmetical methods, applying firstly a combination of the Newton-Raphson and Regula-Falsi methods for the function

$$\Phi(L_{GR}(\lambda_{halfwidth})) = F(L_{GR}(\lambda_{halfwidth})) - \frac{1}{2},$$

with initial value

$$L_0 = \frac{L_G + L_R}{2}$$

and secondly the bisection method. Now we can calculate the FWHM from the expression

$$FWHM = 2|\lambda_{halfwidth} - \lambda_0|$$

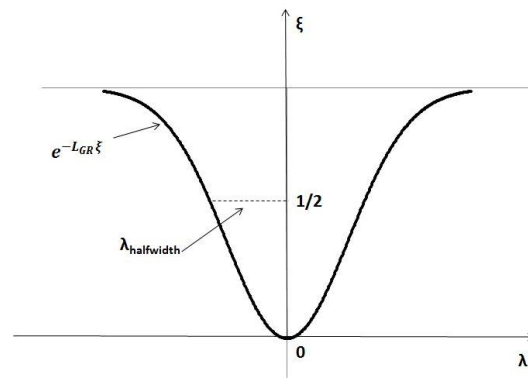


Figure 13. The calculation of the FWHM in the case of the Gauss-Rotation distribution

### Lorentz distribution

In the Lorentz distribution, the main reason of the spectral line broadening is the pressure of the stellar radiation. The Lorentz distribution is given by

$$L_L(\lambda) = \frac{1}{1 + \frac{(\lambda - \lambda_0)^2}{\gamma^2}}$$

where  $\gamma = |\lambda_{HW} - \lambda_0|$  (see figure 14).

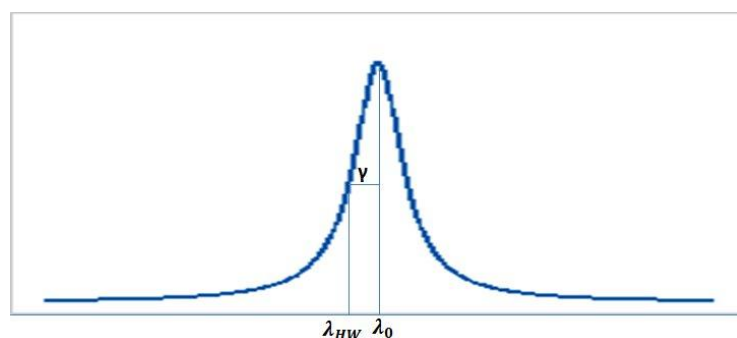


Figure 14. Lorentz distribution

### Voigt distribution

Voigt distribution is the convolution of Gauss and Lorentz distributions. This means that the main reasons of the spectral line broadening are the random motions of the ions as well as the pressure of the stellar radiation.

The convolution of two functions  $f$  and  $g$  is generally given by

$$f * g = \int_{-\infty}^{\infty} f(\tau)g(t - \tau)d\tau$$

In the case of convolution of Gauss and Lorentz distributions we get

$$L_{voigt} = \int_{-\infty}^{\infty} \frac{1}{\sigma\sqrt{2\pi}} e^{-\frac{(\lambda_1-\lambda_0)^2}{2\sigma^2}} \cdot \frac{1}{1 + \frac{(\lambda - \lambda_0 - \lambda_1)^2}{\gamma^2}} d\lambda_1$$

### Calculation of the column density (CD)

An important point of our study is the calculation of the column density from our model (Danezis et al. 2007a).

With the term “column density” we mean the following: Let’s assume a cylinder which has a basis of one  $\text{cm}^2$ . We assume that this cylinder extends from the observer to a density region of matter. We call “column density” of this density region the total number of the particles which are projected on the basis of the cylinder. Obviously, we measure the column density in  $\text{particles}/\text{cm}^2$  (or in  $\text{cm}^{-2}$ ). We can calculate the column density as following: Let’s start from the definition of the optical depth:

$$\tau = \int_0^s k\rho ds$$

where:

$\tau$  is the optical depth (no units),  
 $k$  is the absorption coefficient ( $\text{cm}^2/\text{gr}$ ),  
 $\rho$  is the density of the absorbing region ( $\text{gr}/\text{cm}^3$ ),  
 $s$  is the geometrical depth (cm)

In the model we set  $k = L\Omega$ , so

$$\tau = \int_0^s L\Omega\rho ds$$

where  $L$  is the distribution function of the absorption coefficient  $k$  and has no units,  $\Omega = 1$  and has the units of  $k$  ( $\Omega = 1 \text{ cm}^2/\text{gr}$ ).

We consider that for the moment of the observation and for a specific ion,  $k$  is constant, so  $k$  (and thus  $L$  and  $\Omega$ ) may come out of the integral. So:

$$\tau = L \int_0^s \Omega\rho ds$$

We set

$$\xi = \int_0^s \Omega \rho ds$$

and  $\tau$  becomes

$$\tau = L\xi$$

### ***Absorption lines***

For every one of  $\xi$  along the spectral line (henceforth called  $\xi_i$ ) we have that:

$$\xi_i = \int_0^s \Omega \rho ds \Rightarrow \xi_i = \Omega \int_0^s \rho ds \Rightarrow \frac{\xi_i}{\Omega} = \int_0^s \rho ds$$

We set

$$\sigma_i = \frac{\xi_i}{\Omega} = \int_0^s \rho ds$$

As  $\Omega = 1 \text{ cm}^2/\text{gr}$  contributes only to the units,  $\sigma_i$  takes the value of  $\xi_i$ . For each of  $\lambda_i$  along the spectral line, we extract a  $\sigma_i$  from each  $\xi_i$ . The program we use calculates the  $\xi_i$  for the centre of the line. This means that from this  $\xi_i$  we can measure the respective  $\sigma_i$ .

If we add the values of all  $\sigma_i$  along the spectral line then we have (in  $\text{gr}/\text{cm}^2$ )

$$\sigma = \sum_i \sigma_i$$

which is the surface density of the absorbing matter, which creates the spectral line.

If we divide  $\sigma$  with the atomic weight of the ion which creates the spectral line, we extract the number density of the absorbers, meaning the number of the absorbers per square centimetre ( $\text{cm}^{-2}$ )

$$n = \frac{\sigma}{AW}$$

It is well known, that each absorber absorbs the specific amount of the energy needed for the transition which creates the specific line. So:

The factor  $n * AW$  gr of the ions which create the observed absorption line correspond to a value of energy  $E$ , which is calculated by our model.

The factor  $1 * AW$  gr of the ions corresponds to the energy  $E_i$  that each absorber needs for the transition and is known for each ion.

Thus,

$$\frac{n \cdot AW}{1 \cdot AW} = \frac{E}{E_i} \Rightarrow n = \frac{E}{E_i}$$

This means that the expression  $n = \sigma/AW$  (in  $\text{cm}^{-2}$ ) is arithmetically equal with the  $n = E/E_i$ .

In other words

$$n = \frac{E}{E_i} \text{ in units } \frac{\sigma}{AW}, \text{ which are in } \text{cm}^{-2}$$

This is exactly the column density.

### Emission lines

In the case of emission lines we have to take into account not only  $\xi_e$ , but also the source function  $S$ , as both of these parameters contribute to the height of the emission lines. So in this case we have:

$$S\xi_e = \frac{j}{k} \int_0^s \Omega \rho_e ds$$

where:  $j$  is the emission coefficient  $\left(\frac{\text{erg}}{\text{gr s rad } \text{\AA}}\right)$ ,

$k$  is the absorption coefficient ( $\text{cm}^2/\text{gr}$ )

$\rho_e$  is the density of the emitting region ( $\text{gr}/\text{cm}^3$ )

$s$  is the geometrical depth (cm).

We set

$$k = L\Omega$$

where  $L$  is the distribution function of the absorption coefficient  $k$  and has no units,

$\Omega = 1$  and has the units of  $k$   $\left(\Omega_e = 1 \frac{\text{erg}}{\text{gr s rad } \text{\AA}}\right)$

and

$$j = L_e \Omega_e$$

where  $L_e$  is the distribution function of the emission coefficient  $j$  and has no units,

$\Omega_e = 1$  and has the units of  $j$   $\left(\Omega_e = 1 \frac{\text{erg}}{\text{gr s rad } \text{\AA}}\right)$

As we did before, in the case of the absorption lines, we may consider that  $\Omega$  may come out of the integral.

So:

$$S\xi_e = \frac{j}{k} \int_0^s \Omega \rho_e ds = \frac{L_e \Omega_e}{L \Omega} \int_0^s \Omega \rho_e ds = \frac{L_e \Omega_e}{L \Omega} \Omega \int_0^s \rho_e ds = \frac{L_e \Omega_e}{L} \int_0^s \rho_e ds$$

As in the model we use the same distribution for the absorption and for the emission, ( $L_e = L$ ).

So:

$$S\xi_e = \Omega_e \int_0^s \rho_e ds \Rightarrow \frac{S\xi_e}{\Omega_e} = \int_0^s \rho_e ds$$

We set

$$\sigma_e = \frac{S\xi_e}{\Omega_e} = \int_0^s \rho_e ds$$

As

$$\Omega_e = 1 \frac{\text{erg}}{\text{gr s rad \AA}}$$

contributes only to the units,  $\sigma_e$  takes the value of  $S\xi_e$ .

For each  $\lambda_i$  along the spectral line, we extract a  $\sigma_i$  from each  $S\xi_e$ . The program we use calculates the  $\xi_e$  for the centre of the line and the S. This means that from this  $\xi_e$  and S we can measure the respective  $\sigma_i$ .

If we add the values of all  $\sigma_i$  along the spectral line then we have (in  $\text{gr}/\text{cm}^2$ )

$$\sigma = \sum_i \sigma_i$$

which is the surface density of the absorbing matter, which creates the spectral line.

If we divide  $\sigma$  with the atomic weight of the ion which creates the spectral line, we extract the number density of the emitters, meaning the number of the emitters per square centimetre ( $\text{cm}^{-2}$ )

$$n = \frac{\sigma}{AW}$$

It is well known, that each emitter emits the specific amount of the energy needed for the transition which creates the specific line.

So:

The  $n \cdot AW$  gr of the ions which create the observed absorption line correspond to a value of energy  $E$ , which is calculated by our model.

The  $1 \cdot AW$  gr of the ions corresponds to the energy  $E_i$  that each emitter needs for the transition and is known for each ion.

Thus,

$$\frac{n \cdot AW}{1 \cdot AW} = \frac{E}{E_i} \Rightarrow n = \frac{E}{E_i}$$

This means that the expression  $n = \frac{\sigma}{AW}$  (in  $\text{cm}^{-2}$ ) is arithmetically equal with the

$$n = \frac{E}{E_i}$$

In other words

$$n = \frac{E}{E_i} \text{ in units } \frac{\sigma}{AW}, \text{ which are in } \text{cm}^{-2}$$

This is exactly the column density.

**Notes:**

1. The column density is calculated by the most researchers considering that the observed spectral shape consists of only one absorption component. However, we consider that the observed spectral shape consists of a number of absorption components (DACs/SACs). This means that the calculated values of the column density is likely to be lower than the calculated values by other researchers.

2. Comment (Howarth & Prinja, 1989. *The Astrophysical Journal*, 69, 527, p. 561)

"The accuracy of the quoted column densities depends, of course, on the validity of the models used in the profile fits. Several of our assumptions in this regard are certainly in error (e.g., monotonic velocity law, steady state; Lucy 1983; Owocki, Castor, and Rybicki 1988). For example, Prinja, Howarth, and Henrichs, 1987 obtained two sets of very similar column densities for  $\xi$  Per using two rather different sets of assumptions for line formation. Nonetheless, the models are demonstrably deficient, so our  $N^{\text{H}}$  and  $N^{\text{Fe}}$  data are, strictly, parameters, not measurements".

## The first tests of the line function and the interpolation polynomial

In order to test the validity of our model we perform two tests (Danezis et al. 2007a).

1. We calculated the rotational velocity of the He I absorption line at  $\lambda$  4387.928 Å for five Be stars, using two methods, the classical Fourier analysis and our model. In Fig. 15 we present the five He I  $\lambda$  4387.928 Å fittings for the studied Be stars and the measured rotational velocities with both methods. The rotational velocities that we calculate with both methods are almost the same.

The values of the rotational velocities, calculated with Fourier analysis, sometimes, may present small differences compared to the values calculated with our method, as in Fourier analysis the whole broadening of the spectral lines is assumed to represent the rotational velocity. In contrary, our model accepts that a part of this broadening arises from the random motion of the ions.

We point out that with our model, apart from the rotational velocities, we can also calculate some other parameters as the standard Gaussian deviation ( $\sigma$ ), the velocity of random motions of the ions, the radial velocities of the regions producing the studied spectral lines, the full width at half maximum (FWHM), the optical depth, the column density and the equivalent width.

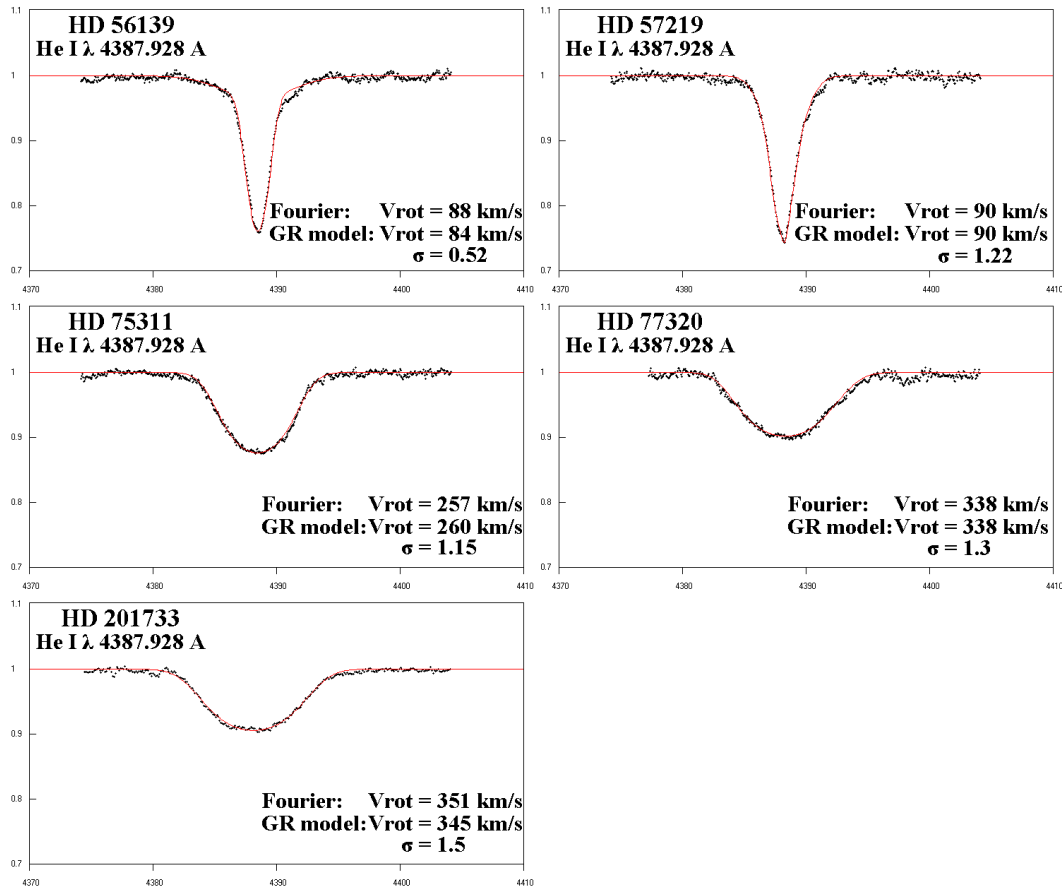


Figure 15. The five He I  $\lambda$  4387.928 Å fittings for the studied Be stars with RG model and the measured rotational velocities with Fourier analysis and RG model. The differences between the observed and the reproduced spectral lines are hard to see, as we have accomplished the best fit (Danezis et al. 2007a).

2. A second test of our model is to calculate the random velocities of the density regions that produce the C IV satellite components of 20 Oe stars with different rotational velocities. The values of the random velocities do not depend on the inclination of the rotational axis. As the ionization potential of the regions that create the satellite components for all the studied stars is the same, we expect similar average values of the random velocities for each component for all the studied stars.

We apply the model on the C IV line profiles of 20 Oe stellar spectra taken with the IUE – satellite (IUE Database <http://archive.stsci.edu/iue>).

We examine the complex structure of the C IV resonance lines ( $\lambda\lambda$  1548.155 Å, 1550.774 Å). Our sample includes the subtypes O4 (one star), O6 (four stars), O7 (five stars), O8 (three stars) and O9 (seven stars). The values of the photospheric rotational velocities are taken from the catalogue of Wilson (1963).

In the study of the C IV spectral lines we detect two components in 9 stars, three in 7 stars, four in 3 stars and five in one star.

In Fig. 16 we present the C IV resonance lines best fit for the star HD 209975.

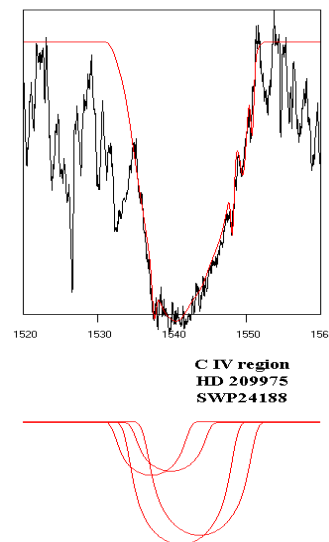


Figure 16. The C IV resonance lines ( $\lambda\lambda$  1548.155, 1550.774 Å) best fit with GR model for the star HD 209975. The analysis of the observed profile to its SACs is presented below the fit (Danezis et al. 2007a).

In Fig. 17 we present the random velocities ( $V_{\text{rand}}$ ) of each SAC as a function of the photospheric rotational velocity ( $V_{\text{phot}}$ ) for all the studied stars.

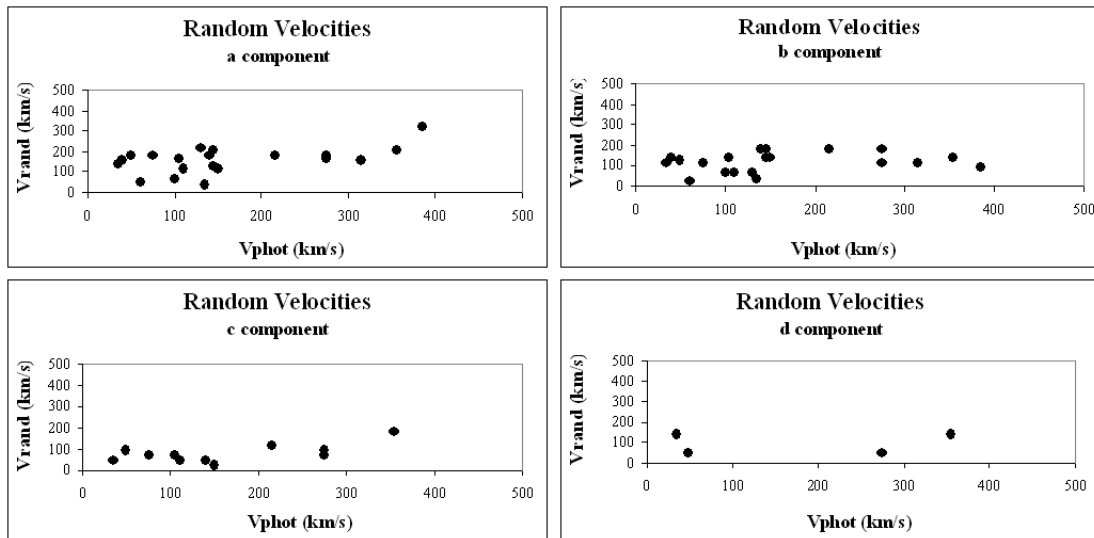


Figure 17. Random velocities ( $V_{\text{rand}}$ ) of the four SACs as a function of the photospheric rotational velocity ( $V_{\text{phot}}$ ) for all the studied Oe stars (Danezis et al. 2007a).

In Fig. 18 we give the relation between the random velocities and the photospheric rotational velocities of the studied stars.

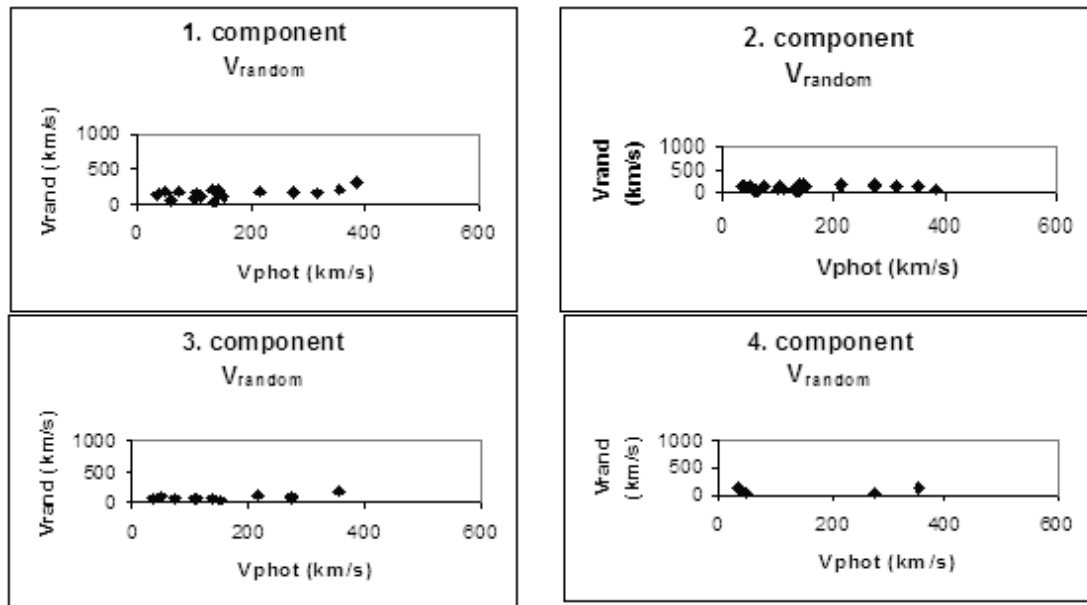


Figure 18. Relation between the random velocities and the photospheric rotational velocities of the studied stars (Danezis et al. 2006).

As we can see the results that arise from the proposed model and are presented in figures 15-18 are in accordance with the classical theory. As it is known, the values of the random velocities do not depend on the value of the inclination of the rotational axis. As the ionization potential of the regions where the SACs are created is the same for all the studied stars, we expect similar average values of the random velocities for each component for all the studied stars, as the velocities calculated with the proposed model. This concurrence is a successful

test for the validity of the proposed model. It is known that the differences between the average values of the random velocities of the SACs arise from the small divergences of the temperature that we can find in each one of the regions that produce the SACs.

### **References**

- Abbott D.C., 1982a, ApJ 259, 282
- Andrillat, Y. and Fehrenbach, Ch.: 1982, A&ASS 48, 93–136.
- Andrillat, Y.: 1983, A&ASS 53, 319–338.
- Antoniou, A. et al. 2007a, uasb.conf, 143
- Antoniou, A. et al. 2007b, uasb.conf, 149
- Antoniou, A. et al. 2007c, uasb.conf, 155
- Antoniou, A. et al. 2007d, AIPC, 938, 194
- Antoniou, A. et al. 2008, POBeo, 84, 443
- Antoniou, A., Danezis, E., Lyratzi, E., Stathopoulos, D., Dimitrijević, M. S. 2011a, BaltA, 20, 548
- Antoniou, A., Stathopoulos, D., Danezis, E., Lyratzi, E. 2011b, BaltA, 20, 572
- Antoniou, A. et al. 2014, AdSpR, 54, 1308
- Barker, P. K., Marlborough, J. M. & Landstreet J. D. 1984, NASCP, 2349, 219
- Barker, P. K., Marlborough, J. M. 1985, ApJ, 288, 329
- Bates, B. & Halliwell, D. R.: 1986, MNRAS, 223, 673
- Bates, B. and Gilheany, S.: 1990, MNRAS 243, 320B.
- Bidelman, W. P., Svolopoulos, S. N. 1960, PASP, 72, 129
- Bosch-Ramon, V. 2013, A&A, 560A, 32
- Capellupo, D. M., Hamann, F. & Barlow, T. A., MNRAS, 444, (2014), 1893.
- Capellupo, D. M., Hamann, F., Barlow, T. A. 2014, MNRAS, 444, 1893.
- Carciofi, A. C. 2011, in IAU Symposium, Vol. 272, Active OB Stars: Structure, Evolution, Mass Loss, and Critical Limits, ed. C. Neiner, G. Wade, G. Meynet, & G. Peters, 325–336
- Cidale, L.S.: 1998, ApJ 502, 824.
- Conti, P. S., & Leep, E. M. 1974, ApJ, 193, 113
- Cranmer, S. R., & Owocki, S. P. 1996, ApJ, 462, 469
- Cranmer, S.R. & Owocki, S.P. 1996, ApJ, 462, 469
- Cranmer, S. R., Smith, M. A. & Robinson, R. D.: 2000, ApJ, 537, 433.
- Crenshaw, D. M., Kraemer, S. B., Boggess, A., Maran, S. P., Mushotzky, R. F., & Wu, C.-C. 1999, ApJ, 516, 750
- Danezis, E.: 1983, The nature of Be stars, PhD Thesis (University of Athens)
- Danezis, E.: 1987, IAU, Colloq. No 92, Physics of Be Stars (Cambridge University Press)
- Danezis, E., Theodossiou, E., Laskarides, P. G. 1991, Ap&SS, 179, 111
- Danezis, E., Nikolaidis, D., Lyratzi, V., Stathopoulou, M., Theodossiou, E., Kosionidis, A., Drakopoulos, C., Christou, G., Koutsouris, P. 2003e, Ap&SS, 284, 1119

- Danezis, E., Antoniou, A., Lyratzi, E., Theodossiou, E., Stathopoulou, M., Nikolaidis, D., Drakopoulos, C., Soulikias, A., Koutroumanou, M. 2003a, POBeo, 76, 175
- Danezis, E., Lyratzi, E., Nikolaidis, D., Stathopoulou, M., Theodossiou, E., Drakopoulos, C., Soulikias, A., Antoniou, A. 2003b, POBeo, 76, 179
- Danezis, E., Popović, L. Č., Lyratzi, E., Dimitrijević, M. S. 2006, AIPC, 876, 373
- Danezis, E., Nikolaidis, D., Lyratzi, E., Popovic, L. C., Dimitrijevic, M. S., Antoniou, A., Theodosiou, E. 2007a, PASJ, 59, 827
- Danezis, E., Antoniou, A., Lyratzi, E., Popović, L. Č., Dimitrijević, M.S., Nikolaidis, D. 2007b, AIPC, 938, 119
- Danezis, E.; Lyratzi, E.; Popović, L. Č.; Dimitrijević, M. S.; Antoniou, A. 2008, AIPC, 1058, 305
- Danezis, E., Lyratzi, E., Popović, L. Č., Dimitrijević, M. S., Antoniou, A. 2009, NewAR, 53, 214
- Danezis, E., Lyratzi, E., Antoniou, A., Popović, L. Č., Dimitrijević, M. S. 2010a, MSAIS, 15, 13
- Danezis, E., Lyratzi, E., Popovic, L. C., Dimitrijevic, M. S., Antoniou, A. 2010b, ASPC, 424, 305
- Drechsel, H. & Rahe, J. 1982, A&A, 106, 70
- Feldmeier, A., & Shlosman, I. 1999, ApJ, 526, 344
- Foltz, C., Wilkes, B., Weymann, R., Turnshek, D. 1983, PASP, 95, 341.
- Foltz, C. B., Weymann, R. J., Morris, S. L., & Turnshek, D. A. 1987, ApJ, 317, 450
- Foltz, C. B., Chaffee, F. H., Hewett, P. C., Weymann, R. J., Morris, S. L. 1990, BAAS, 2, 806.
- Friend D.B., Abbott D.C., 1986, ApJ 311, 701
- Fullerton, A. W., Massa, D. L., Prinja, R. K., Owocki, S. P. & Cranmer, S. R.: 1997, A. & A., 327, 699.
- Fullerton, A. W.; Petit, V., Bagnulo, S., Wade, G., A. 2011, IAUS, 272, 182
- Garmany, C. D., Olson, G. L., Conti, P. S., van Steenberg, M. E. 1981, ApJ, 343, 426
- Gathier, R., Lamers H. J. G. L. M., Snow, T. P. 1981, ApJ, 247, 173
- Gilheany, S., Bates, B., Catney, M.G. and Dufton, P.L.: 1990, Ap&SS 169, 85G.
- Grady, C. A., Bjorkman, K. S., Snow, T. P. 1987, ApJ, 320, 376
- Grady, C.A., Sonneborn, G., Chi-chao, Wu., Henrichs, H.F., 1987. ApJ Suppl. 65, 673
- Grundstrom, E. D., McSwain, M. V., Aragona, C., et al. 2011, Bulletin de la Societe Royale des Sciences de Liege, 80, 371
- Hamann, F., Chartas, G., McGraw, S., Rodriguez Hidalgo, P., Shields, J., Capellupo, D., Charlton, J. & Eracleous, M., 2013, MNRAS, 435, 133.
- Harnden F.R. Jr., Branduardi G., Gorenstein P., 1979, ApJ 234, 51
- Hazard, C., McMahan, R. G., Webb, J. K., Morton, D. C. 1987, ApJ, 323, 263.
- Heap, S. R. et al. 1979, Nature, 275, 15
- Heap, S. R. 1986, ESASP, 263, 291
- Hearn, A. G. 1979, IAUS, 83, 169
- Hearn, A. G. 1981, ASSL, 89, 125

- Henrichs, H. F. (1984) Proceedings of the 4th European IUE Conference, Rolfe, E., Battrick, B. (Eds.), ESA SP-218, p. 43
- Henrichs, H. 1988, NASSP, 497, 199
- Henrichs H.F., Kaper L., Zwarthoed G.A.A., 1988, in A Decade of UV Astronomy with the IUE Satellite (ESA SP-281), Vol.2, p.145
- Henrichs, H. F., Kaper, L., & Nichols, J. S. 1994, A&A, 285, 565
- Hewett, P. C, Foltz, C. B. 2003, 125, 1784
- Hillier, D.J. & Miller, D.L. 1999, ApJ, 519, 354
- Kaper, L., Henrichs, H. F. 1994, Ap&SS, 221, 115
- Kaper, L., Henrichs, H.F., Nichols, J.S., Snoek, L.C., Volten, H., Zwarthoed, G.A.A., 1996. A&A Suppl. 116, 257
- Kaper, L., Henrichs, H.G., Fullerton, A.W., Ando, H., Bjorkman, K.S., Gies, D.R., Hirata, R., Dambe, E., McDavid, D., Nichols, J.S., 1997. A&A 327, 281
- Kaper, L., Henrichs, H.F., Nichols, J.S. and Telting, J.H.: 1999, A&A 344, 231.
- Kee, N., Owocki, S., Townsend, R., & Muller, H.-R. 2014, ArXiv e-prints, arXiv:1412.8511
- Klement, R. et al. 2017, A&A, 601A, 74
- Krautter, J., Vogt, N., Klare, G., Wolf, B., Duerbeck, H. W., Rahe, J., & Wargau, W. 1981, A&A, 102, 337
- Kriss, G. A., Green, R. F., Brotherton, M., et al. 2000, ApJ, 538, L17
- Krolik, J. H. 1999, Active Galactic Nuclei: From the Central Black Hole to the Galactic Environment
- Kroll, P., & Hanuschik, R. W. 1997, in Astronomical Society of the Pacific Conference Series, Vol. 121, IAU Colloq. 163: Accretion Phenomena and Related Outflows, ed. D. T. Wickramasinghe, G. V. Bicknell, & L. Ferrario, 494
- Labadie-Bartz, J. et al. 2017, AJ, 153, 252
- Lamers, & A. Sagar, ASP Conf. Ser., 204, 3
- Lamers, H. J. G. L. M. & Snow, T. P. 1978, ApJ, 219, 504
- Lamers, H.J.G.L.M., Gathier, R. and Snow, T.P.: 1982, ApJ 258, 186.
- Lamers, H.J.G.L.M., Snow, T.P., de Jager, C., Langerwerf, A., 1988. ApJ 325, 342
- Lamers, H. J. G. L. M., & Cassinelli, J. P. 1999, Introduction to Stellar Winds
- Lee, U., Osaki, Y., & Saio, H. 1991, MNRAS, 250, 432
- Lobel, A., & Blomme, R. 2008, ApJ, 678, 408
- Lucy, L. B., & Solomon, P. M. 1970, ApJ, 159, 879
- Lucy, L. B., White, R. L. 1980, ApJ. 241, 300
- Lucy, L. B. ApJ. 1984, 284, 351
- Lyratzi, E., Danezis, E., Stathopoulou, M., Theodossiou, E., Nikolaidis, D., Drakopoulos, C., Soulikias, A. 2003, POBeo, 76, 27
- Lyratzi, E., Danezis, E. 2004, AIPC, 740, 458
- Lyratzi, E., Danezis, E., Popovic, L. C., Dimitrijevic, M. S., Nikolaidis, D., Antoniou, A. 2007, PASJ, 59, 357
- Lyratzi, E., Popovic, L. C., Danezis, E., Dimitrijevic, M. S., Antoniou, A. 2009, NewAR, 53, 179.

- Lyratzi, E., Danezis, E., Popovic, L. C., Dimitrijevic, M.S., Antoniou, A. & Stathopoulos, D., 2010, MSAIS, 15, 161.
- Lyratzi, E., Danezis, E., Popovic, L. C., Antoniou, A., Dimitrijevic, M. S., Stathopoulos, D. 2011, BaltA, 20, 448.
- Markova, N.: 2000 A&AS 144, 391.
- Martens, P. C. H. 1979, Astr. Ap. 65, 223
- Massa, D., Fullerton, A. W., Nichols, J. S., et al. 1995, ApJ, 452, L53
- Mathews, W. G. 1986, ApJ, 305, 187
- Matthews, J. H., Knigge, C., Long, K. S., Sim, S. A., Higginbottom, N., Mangham, S. W., 2016, MNRAS, 458, 29.
- Mauche, C. W., Raymond, J. C. 1997, in Cosmic winds and the heliosphere. Edited by J.R. Jokipii, C.P. Sonett, and M.S. Giampapa. Tucson: University of Arizona, 1997, p.111
- McCandliss, S.R. 1988, PhD Thesis, Colorado Univ., Boulder
- McKee, C. F. & Tarter, C. B., 1975, ApJ, 202, 306.
- Misawa, T., Inada, N., Oguri, M., Gandhi, P., Horiuchi, T., Koyamada, S. & Okamoto, R., 2014, ApJ, 794, 20.
- Moffat, A.F.J., et al. 1988, ApJ, 334, 1038
- Moffat, A. F. J. 2008, in Proc. Clumping in hot-star winds, eds. W.-R. Hamann, A. Feldmeier, & L. M. Oskinova, 17
- Mullan, D. J. 1984a, ApJ, 283, 303
- Mulan, D.J.: 1984b, ApJ 284, 769.
- Mulan, D.J.: 1986, A&A 165, 157.
- Murray N., Chiang J., Grossman S. A., Voit G. M. 1995 ApJ, 451, 498.
- Negueruela, I., Steele I. A., & Bernabeu, G. 2004, AN, 325, 749
- Nelson, G., & Hearn, A. G. 1978, Asatr. Ap. 65, 417
- Owocki, S. P., and Rybicki, G. B. (1984) Astrophys. J. 284, 337.
- Owocki, S. P., & Rybicki, G. B. 1985, ApJ, 299, 265
- Owocki, S. P., & Rybicki, G. B. 1986, ApJ, 309, 127
- Owocki, S. P. 1990, RvMA, 3, 980
- Owocki, S. P., & Rybicki, G. B. 1991, ApJ, 368, 261
- Owocki, S. P., Cranmer, S. R., & Fullerton, A. W. 1995, ApJ, 453, L37
- Owocki, S. P., & Cohen, D. H. 2006, ApJ, 648, 565
- Pauldrach A.W.A., Puls J., Kudritzki R.P., 1986, A&A 164, 86
- Pauldrach, A., Puls, J., Kudritzki, R. P., Mendez, R. H., Heap, S. R. 1988, A&A, 207, 123
- Pauldrach A.W.A., Kudritzki R.P., Puls J., Butler K., Hunsinger J., 1994, A&A 283, 525
- Porter, J. M., & Rivinius, T. 2003, PASP, 115, 1153
- Prinja, R. K. A&A, 232, 119
- Prinja, R. K., Howarth, I. D. 1986, ApJS, 61, 357
- Prinja, R. K., Howarth, I. D., Henrichs, H. F. 1987, ApJ, 317, 389
- Prinja, R. K., Howarth, I. D. 1988, MNRAS, 233, 123
- Prinja, R. K., Massa, D., & Fullerton, A. W. 2002, A&A, 388, 587

- Proga, D., Kallman, T.R., Drew, J. E., Hartley, L. E. 2002, ApJ, 572, 382
- Proga, D. 2005, ASPC, 330, 103
- Proga, D. 2007, ASPC, 373, 267
- Proga, D., Jiang, Y.-F., Davis, S.W., Stone, J. M., Smith, D. 2014, ApJ, 780, 51
- Proga, D., Waters, T. 2015, ApJ, 804, 137
- Puebla et al. 2007, AJ, 134, 1923
- Puebla, et al. 2011, ApJ, 736, 17
- Rauw, G., Nazé, Y., Marique, P. X., et al. 2007, IBVS, 5773, 1
- Reichard, T. A., Richards, G. T., Hall, P. B., Schneider, D. P., VandenBerk, D. E., Fan, X., York, D. G., Knapp, G. R., Brinkmann, J. 2003, AJ, 126, 2594.
- Rivinius, Th., Stahl, O., Wolf, B., Kaufer, A., Gäng Th., Gummersbach, C.A., Jankovics, I., Kovács, J., Mandel, H., Peitz, J., Szeifert, Th. and Lamers, H.J.G.L.M.: 1997, A&A 318, 819.
- Rivinius, T., Baade, D., Stefl, S., et al. 1998, A&A, 333, 125
- Rivinius, T., Carciofi, A. C., & Martayan, C. 2013, A&A Rev., 21, 69
- Robert, C. 1992, PhD Thesis, Universite de Montreal
- Rogerson, J. B., Jr, and Lammers, H. J. G. L. M. (1975) Nature 256, 190.
- Runacres, M. C., & Owocki, S. P. 2002, A&A, 381, 1015
- Rybicki, G. B., Owocki, S. P., & Castor, J. I. 1990, ApJ, 349, 274
- Sahade, J., Brandi, E. & Fontela, J.M.: 1984, Astron. Astrophys. Supplement, 56, 17.
- Sahade, J. & Brandi, E.: 1985, Rev. Mex. 10, 229.
- Sako, M. et al. 2001 A&A 365, 168
- Scargle, J. D., Caroff, L. J., Noerdlinger, P. D. 1970, ApJ (Letters), 161, 115.
- Schumann, J.D. & Seggewiss, W. 1975, IAUS, 67, 299
- Simon, K. P., Gruschinske, J., Haman, W. R., Hunger, K., Kudritzki, R. P. 1979, IUE1, symp, 354S
- Slettebak, A., 1988. PASP 100, 770.
- Snow, T. P. 1981, ApJ, 251, 139
- Stathopoulos, D., Danezis, E., Lyratzi, E., Antoniou, A., Tzimeas, D., 2015, JApA, 36, 495.
- Stathopoulos, D., E., Lyratzi, E., Danezis, Antoniou, A., Tzimeas, D., 2017, EPJD, accepted for publication.**
- Takeuchi, S., Ohsuga, K. & Mineshige, S., 2013, PASJ, 65, 88.
- Turnshek, D. A., 1984, ApJ, 280, 51.
- Turnshek, D. 1986, Broad Absorption Line QSOs. Symposium - International Astronomical Union, 119, 317
- Turnshek, D. A., Grillmair, C. J., Foltz, C. B., Weymann, R. J. 1988, ApJ, 325, 651.
- Underhill, A.B., 1975. ApJ 199, 691
- Vardya, M. S., Narlikar, J. V., Underhill, A., B., Doazan, V., Anson F., F.1982, BASI, 10, 256
- Vilkoviskij, E. Y., Yefimov, S. N., Pavlova, L. A., Baturina, E. B. 2003, A&AT, 22, 219
- Vink, J. S. 2000, PhDT, 45V
- Voit, G. M., Weymann, R. J., Korista, K. T. 1993, ApJ, 413, 95.

- Waldron, W.L., Klein, L., Altner, B., 1992. ASP Conf. Series 22, 181
- Waldron, W.L., Klein, L., Altner, B., 1994. ApJ 426, 725
- Walter, R., & Zurita Heras, J. 2007, A&A, 476, 335
- Waters, T. & Proga, D. 2016, MNRAS, 460, 79
- Weymann, R. J., Morris, S. L., Foltz, C. B., & Hewett, P. C. 1991, ApJ, 373, 23
- Willis, A. J., van der Hucht, K. A., Conti, P. S., Garmany, C. D., 1986, A&AS, 63, 417
- Willis, A. J., Garmany, C. D. 1987, ASSL, 129, 157
- Wilson, R. E., 1963, General Catalogue Of Stellar Radial Velocities, Washington, Carnegie Institution of Washington Publication 601
- Wolf, B., Stahl, O., Fullerton A.W., 1998, Variable and Non-spherical Stellar Winds in Luminous Hot Stars, Lecture notes in Physics, IAU Coll.no. 169
- Zorec, J. & Briot, D. 1997, A&A, 318, 443